RESEARCH ARTICLE | APRIL 21 2023

An experimental and analytical study of wind turbine wakes under pressure gradient

Arslan Salim Dar ; Abraham Starbuck Gertler ; Fernando Porté-Agel

Physics of Fluids 35, 045140 (2023)
https://doi.org/10.1063/5.0145043

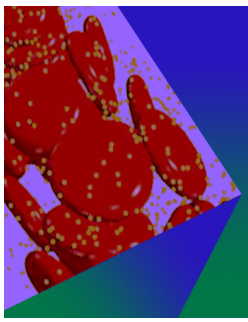

Physics of Fluids ARTICLE scitation.org/journal/phf

An experimental and analytical study of wind turbine wakes under pressure gradient

Cite as: Phys. Fluids **35**, 045140 (2023); doi: 10.1063/5.0145043
Submitted: 2 February 2023 · Accepted: 4 April 2023 ·
Published Online: 21 April 2023

Arslan Salim Dar, Abraham Starbuck Gertler, and Fernando Porté-Agel[a)]

AFFILIATIONS

Wind Engineering and Renewable Energy Laboratory (WIRE), École Polytechnique Fédérale de Lausanne (EPFL), 1015-Lausanne, Switzerland

[a)]Author to whom correspondence should be addressed: fernando.porte-agel@epfl.ch

ABSTRACT

This work is dedicated to the systematic investigation of wind turbine wakes under the effect of pressure gradients. Wind tunnel experiments are carried out with a wind turbine positioned on straight ramps of increasing angle such that it experiences an approximately linear flow speed-up/slow-down from the induction region into the far wake. Fifteen ramp angles are studied: 7 favorable (FPG), 7 adverse (APG), and 1 zero pressure gradient. The wake center is shown to follow the base flow streamline originating from a virtual turbine hub height. A quasi-linear relationship between the pressure gradient and near wake length is demonstrated. Far wake characteristics, such as the recovery of the wake center velocity deficit and wake growth rate, are observed to systematically vary with the pressure gradient. The wake recovery rate increases (decreases) with the increase in the FPG (APG), and the wake growth rate shows a linear increase from most favorable to most adverse pressure gradient. The turbine power coefficient decreases significantly with increasing APG to a greater degree than the increase in power coefficient under FPG. The engineering approach of superposing the wake deficit predicted by the standard Gaussian model on the modified base flow is shown to work for very moderate pressure gradients. In light of this, a threshold in terms of flow speed-up/slow-down along the wake trajectory is established, below which the engineering approach can be reasonably employed. Finally, a physics-based model for wakes under the pressure gradient is tested. A new theoretical relation for near wake length under the pressure gradient is proposed. Using the theoretical near wake length, the pressure gradient model predicts the turbine wakes for all cases with good accuracy and shows a significant improvement from the engineering approach.

I. INTRODUCTION

Global wind energy capacity has grown exponentially over the last few decades, with a cumulative installed capacity of 837 GW at the end of 2021.[1] Despite this growth, it is estimated that to achieve the goal of net zero emissions by 2050, the yearly new wind energy installations need to be tripled by 2030 compared to those in 2020.[1] Although wind energy has grown significantly—making it one of the cheapest available energy sources today,[2] even bigger challenges lie ahead if we are to achieve the ambitious goals set to tackle climate change. According to Veers *et al.*,[3] we need to address three grand challenges in the science of wind energy to access its full potential. The first of these challenges is to improve our understanding of the complicated physical interactions between atmospheric flows and wind farms, whereas the other two challenges are concerned with the aerodynamics of large wind turbines and grid integration of large wind farms. The fact that within wind farms most wind turbines operate in the wake of others makes things even more challenging. Turbine wakes, characterized by low velocity and high turbulence, depend mainly on the characteristics of the local flow and turbine operating conditions. A large body of literature exists which aims at understanding the interactions between wind turbines and surrounding flows under a range of different flow and turbine operating conditions.[4,5]

For wind turbines installed onshore, the likelihood is high that wind farms are sited in complex terrain or heterogeneous surface roughness conditions.[6] Changes in terrain elevation or surface roughness have significant consequences for the boundary layer flow developing on top of it, inducing variations in flow shear, generating localized flow features and imposing localized pressure gradient. Understanding how wind turbines interact with such complicated flows, and more importantly, how those interactions differ from the ones in flat terrain is of paramount importance. This is due to the fact that most existing literature deals with wind turbines on flat terrain,

and to what extent that knowledge can be extrapolated to a complex one remains to be understood.

Recent years have seen an increased interest in wind turbine wakes and power performance in complex terrain from the wind energy community. Tian *et al.*[7] performed an experimental study of a wind farm sited on a two-dimensional gentle hill and showed that the hilltop was the ideal location for power production, whereas turbines sited on the up- or down-hill slopes produced comparatively less power due to the sheltering effect and wake of the hill, respectively. Hyvärinen and Segalini[8] investigated the power and thrust coefficients of wind turbines sited on periodic sinusoidal hills. They showed that the thrust and power coefficients remained comparable between a turbine sited on flat and sinusoidal hills. For two aligned turbines, they observed that the in-wake turbine performed better in the presence of hills than in the flat case. Liu and Stevens[9] showed that the power performance of a turbine sited on a two-dimensional hill depends on the relative height of the turbine with respect to the hill. For a wind farm sited across the hill, the turbines located on the leeward side of the hill suffered in terms of power production. Atmospheric stability has also been shown to have a strong effect on wind turbine power production in complex terrain.[10–12] More recently, Troldborg *et al.*[13] showed that complex terrain can change the power curve of a wind turbine compared to a flat terrain due to a change in the turbine induction.

For wind turbine wakes in complex terrain, several studies have investigated how the terrain affects some important wake characteristics. Recovery of the wake velocity deficit is an important factor in determining optimal inter-turbine spacing within a wind farm. Most studies have shown that turbine wakes recover faster in complex terrain compared to what is normally reported in a flat one.[14–20] This observation is attributed to the terrain enhanced turbulence production, which leads to higher entrainment of energy into the wake, and thus, faster recovery. An associated characteristic of the wake is its expansion in the cross-stream direction, which has also been shown to be higher in steep terrain.[17–19] The terrain is also known to affect the trajectory of the wake. Menke *et al.*[21] found that the wake trajectory is dependent on atmospheric stability in a complex terrain. They showed that the turbine wake follows the terrain in stable conditions, deflects upward in unstable conditions, and propagates horizontally under neutral conditions. Barthelmie and Pryor,[22] however, made an opposite observation in the same terrain and associated the discrepancy with the observations of Menke *et al.*[21] to the downstream distance over which the wake trajectory was followed. Liu *et al.*[23] performed large eddy simulation of wind turbine wake over two- and three-dimensional hills and evaluated different strategies of superposing a turbine wake on a hill. They found that the strategy of following the flow streamline originating from turbine hub height works best. Dar and Porté-Agel[17] showed that for a turbine sited on an escarpment, the vertical velocity imposed by the surrounding flow affects the wake trajectory. They also showed that the meandering of the wake is dependent on the turbulence intensity induced by the terrain.[17,24] Moreover, atmospheric stability has also been shown to influence the development of turbine wakes in complex terrain.[10,25]

Changes in terrain elevation or surface roughness conditions also result in localized pressure gradients. The effect of the pressure gradient on the development of wakes is a classical problem of fluid mechanics. Hill *et al.*[26] investigated the effect of moderate pressure gradients on the wake of an obstructive rectangular bar. They showed that adverse pressure gradients (APGs) can cause the wake deficit recovery to slow down and wake width to grow rapidly. Additionally, they developed a simple model to capture these effects. Nakayama[27] performed a combined study of pressure gradient and streamline curvature on the wake of a two-dimensional airfoil-like thin plate. They showed that both the mean flow and turbulence quantities are affected by the pressure gradient and streamline curvature. Liu *et al.*[28] performed experiments to investigate a planar wake exposed to constant adverse and favorable pressure gradients. They showed that even moderate pressure gradients can affect the wake deficit and growth rate. In addition, they found that the wake deficit remains self-similar under pressure gradient. A follow-up study was performed to investigate the similarities and differences between symmetric and asymmetric wakes under pressure gradient.[29] Among other things, they showed that the ratio of wake deficit to its width remained insensitive to the imposed pressure gradient. Rogers[30] performed direct numerical simulations of turbulent planar wakes. They found a universal profile for the mean wake velocity deficit and observed that the response of turbulence quantities to the pressure gradient was smaller than that of the mean flow. More recently, Shamsoddin and Porté-Agel[31] proposed an analytical model for planar wakes and validated it with the experimental data of Liu *et al.*[28] All of these studies consider turbulent planar wakes, where favorable (adverse) pressure gradients have been shown to enhance (slow-down) the wake deficit recovery and reduce (increase) the wake expansion rate.

Wind turbine wakes, on the other hand, are three-dimensional with a reasonable axisymmetry in the cross-stream plane. The effect of the terrain-induced pressure gradient on wind turbine wakes has been explored in some recent studies. Shamsoddin and Porté-Agel[32] proposed an analytical model for turbulent axisymmetric wakes and validated it with their large-eddy simulations. They then applied this model to the wake of a wind turbine located upstream of a hill and combined it with the streamline curvature caused by the hill.[33] They also identified two regions of flow over a hill corresponding to adverse and favorable pressure gradients and showed how the recovery of the wake depends on its position relative to the hill. Cai *et al.*[34] performed an experimental study of wind turbine wake under the pressure gradient. They placed a turbine at the edge of a ramp and varied the imposed pressure gradient by altering the ramp slopes. They tested the model of Shamsoddin and Porté-Agel[32] and found good agreement with the data. Furthermore, they investigated the effect of the pressure gradient induced change in velocity on the power output of the turbine.

Analytical modeling of wake velocity deficit is one of the most active areas of research in the wind energy community, as it provides computationally cheap estimation of turbine wakes with a reasonable accuracy. Such models are widely used in the industry during the layout optimization phase of wind farm planning, as they enable the evaluation of multiple layouts and wind directions in relatively short time. For a detailed review of analytical wake models, the reader is referred to Refs. 4, 35, and 36. Some notable mentions in this context are the Jensen model,[37] Frandsen model,[38] and the Bastankhah and Porté-Agel model[39] (also known as the Gaussian model). Most analytical models are derived using mass and/or momentum conservation under the assumption of a zero pressure gradient (ZPG). The Gaussian model[39] derives an algebraic equation for the streamwise evolution of the maximum wake velocity deficit and uses the self-similarity of the wake to produce the velocity deficit profiles. This self-similarity of the

turbine wake has been verified experimentally and numerically for flat and complex terrains.[17,39–41]

For wind turbines in complex terrain, the assumption of a zero pressure gradient does not hold. Nevertheless, several studies have tried to adapt the Gaussian model[39] for the application in complex terrain. Brogna *et al.*[42] proposed a modified Gaussian model for their layout optimization study. For different turbines, the local base flow (flow without turbine) velocity at a given turbine position was used to account for topography effects. More recently, Farrell *et al.*[43] also proposed an adapted formulation of the Gaussian model for application in complex terrain. They made the reference velocity in the Gaussian model spatially variable throughout the wake, thereby claiming to improve over the approach of Brogna *et al.*[42] They, however, acknowledged that the approach of adapting Gaussian model to varying base flow velocity violates the conservation of streamwise momentum, as the underlying model is derived under the assumption of the zero pressure gradient. Such approaches of superposing a Gaussian model on a varying base flow can at best be considered engineering approaches and their simplicity makes them suitable for industrial applications. A physics based model for wind turbine wakes under the pressure gradient has been proposed by Shamsoddin and Porté-Agel.[32] This model accounts for the effect of an arbitrary imposed pressure gradient on the far wake evolution of an axisymmetric wake. More recently, Dar and Porté-Agel[44] extended the model of Shamsoddin and Porté-Agel[32] to account for the effect of an imposed pressure gradient in the near wake as well.

The current work is inspired by the need for a systematic study of wind turbine wakes under a range of terrain-induced pressure gradients. We have performed wind tunnel experiments with a miniature wind turbine, where the pressure gradients are induced by means of constant slope ramps with different inclination angles. The turbine is placed such that the induction region, near wake and far wake are all exposed to an approximately constant flow acceleration or deceleration caused by the pressure gradient. The objectives of this study are threefold:

1. To understand systematically how some important wake characteristics such as its recovery, expansion, turbulence quantities, and near-to-far wake transition change across a range of imposed pressure gradients.
2. To define a threshold imposed pressure gradient beyond which the simplified engineering approach of superposing a wind turbine wake obtained from a zero pressure gradient model on a spatially varying base flow velocity does not work.
3. To demonstrate how a physics-based analytical model designed for wakes under the pressure gradient can improve the wake deficit prediction, when the simplified engineering approach fails.

The rest of the article is structured as follows: the experimental setup and results are presented in Sec. II, the analytical modeling approaches are described and compared in Sec. III, and finally, a summary of the work along with some concluding remarks is given in Sec. IV.

II. EXPERIMENTS

A. Setup

The experiments are performed in the closed-loop boundary layer wind tunnel at the WiRE laboratory of EPFL. It is a low-speed wind tunnel driven by a 130 kW fan, with an area contraction ratio of 5:1 at the inlet and a test section of dimensions $28 \times 2.56 \times 2$ m^3 (length $\times$ width $\times$ height). The free-stream turbulence intensity in the test section is typically less than 1%. This is achieved by conditioning the flow through a series of honeycomb meshes and mesh screens before the beginning of the contraction. In addition, the area contraction before the inlet further helps to create a less turbulent and uniform flow at the inlet. A zero pressure gradient boundary layer is developed in the wind tunnel with the adjustment of the ceiling height and width of the walls.

The miniature wind turbine used in this study is a three-bladed horizontal axis turbine developed at the WiRE lab. It is a scaled-down version of the WiRE-01 turbine,[45] where the scaling ratio is 1:1.43 between the scaled-down and original turbine. Dar *et al.*[18] characterized the power and thrust coefficients of the scaled-down turbine and showed that scaling-down the turbine does not influence its performance as long as the Reynolds number is comparable between the original and scaled-down turbines. The hub height z_h and rotor diameter d of the miniature turbine are 8.75 and 10.5 cm, respectively. The rotor is manufactured through 3D-printing using a liquid photopolymer resin material. The rotor is mounted on a direct current motor (model: DCX10L) and controlled using a servo controller (model: ESCON 36/2 DC).

We use linear ramps, where the slope of the ramps is varied between 0° and 13.1° to impose a range of pressure gradients. In total 15 different pressure gradient cases are studied: one for the zero pressure gradient, and seven each for the favorable and adverse pressure gradients. The ramps are 1.35 m (13d, where d is the rotor diameter) in length, 2.5 m in width, and their heights are 0 mm (0 d, 0°), 35 mm (1/3 d, 1.5°), 52 mm (1/2 d, 2.2°), 79 mm (3/4 d, 3.3°), 105 mm (1 d, 4.4°), 157 mm (1.5 d, 6.6°), 210 mm (2 d, 8.8°), and 315 mm (3 d, 13.1°). In the favorable pressure gradient (FPG) cases, the ramps have a positive slope and the turbine is placed at a horizontal distance of 2.5d from the front edge of the ramp, whereas in the adverse pressure gradient (APG) cases, the ramps have a negative slope and the turbine is placed at a horizontal distance of 4d from the front of the ramp. The turbine streamwise position is chosen to distance it from the effect of ramp edges and to position the turbine and wake in a region of approximately constant pressure gradient. The ramp edges were smoothed out with tape to reduce the effects of sharp convex corners. In all cases the turbine tower is pitched to align the rotor with the incoming base flow angle at the hub height. This choice was made to avoid effects of a rotor tilted relative to the flow, so to better isolate the effect of pressure gradient.

A two-dimensional two-component (2D2C) particle-image velocimetry (PIV) system is used to capture flow measurements in a vertical (xz) plane passing through the turbine centerline. Flow measurements are taken with and without the turbine to characterize the wake and base (without turbine) flow, respectively. The PIV system is composed of one sCMOS camera (2560×2160 pixels) with a 50 mm lens; a 425 mJ double-pulsed Nd:YAG laser (Litron lasers, Nano TRL 425–10) at a wavelength of 532 nm; and a programable timing unit (LaVision, PTU-v9). The measurements are captured at a sampling rate of 10 Hz, where 1000 instantaneous fields are used (except for one case, where 750 fields are used) to obtain time averaged flow statistics. The size of the field-of-view (FOV) is $7.5d \times 6.3d$ with a spatial resolution of 0.024d. The flow is seeded with olive oil droplets of several micrometers in diameter through a slot near the inlet of the test section. A sketch of the experimental setup is shown in Fig. 1.

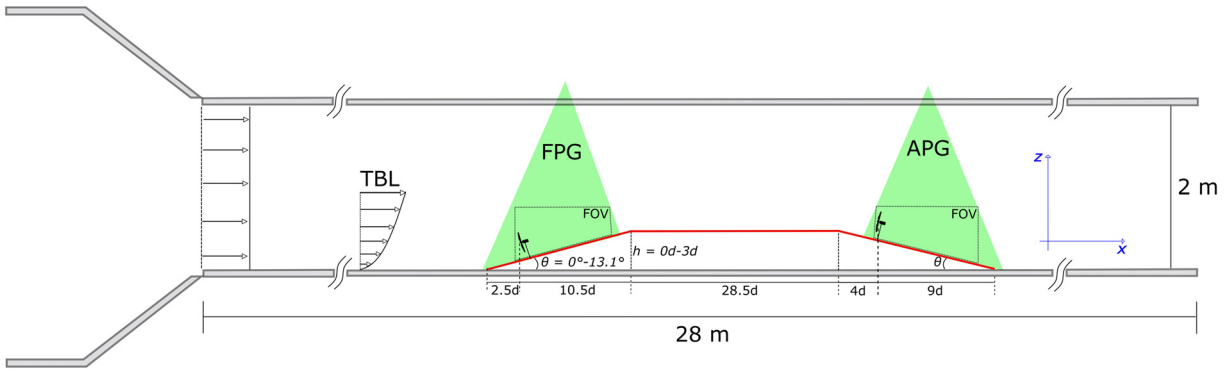

FIG. 1. Schematic representation of the experimental setup (not to scale).

A double-pass reducing size interrogation window of 64×64 pixels and 32×32 pixels with a 75% overlap between consecutive windows is used to perform image post-processing. Bad vectors from the correlation are removed using an outlier detection method, where the maximum uncertainty in the mean flow is estimated to be around 0.06 m s^{-1} based on a correlation statistics approach.[46]

The power produced by the turbine P is measured by multiplying the shaft torque Q of the turbine by its rotational speed Ω. The shaft torque is estimated by multiplying the torque constant K of the DC motor by the generated current I and adding to it the frictional torque Q_f. The detailed procedure for power measurements is described by Bastankhah and Porté-Agel.[45] The power coefficient C_P is estimated using the following relation: $C_P = \frac{P}{1/2\rho A U_r^3}$, where ρ is air density, A is the rotor swept area, and U_r is the rotor equivalent velocity at the turbine position.

Although a natural boundary layer can develop on the smooth wind tunnel floor due to its length,[17] in the current work, we facilitate the development of the boundary layer to further increase its height. We place a picket fence (10 cm in length and 5 cm in height, with spikes of 3 cm in length) at the inlet of the test section and cover the floor of the wind tunnel with double-rolled chains at a streamwise spacing of 40 cm. This is done to increase the boundary layer height such that it is more than twice the height of the ramp in the most extreme case. The inlet velocity of the test section is varied such that the turbine hub height velocity is similar in all cases. The hub height velocity is in the range of 6.26–6.73 m s^{-1}, except for one case where it is 5.96 m s^{-1}. This is done to achieve a comparable Reynolds number ($Re_d = \frac{U_h d}{\nu}$, where ν is the kinematic viscosity of air) in all the cases, which is found to be in the range of 42 500–48 000 in all the cases. Although the Reynolds number in the wind tunnel experiments is smaller than the one for the utility-scale wind turbines, it is close to the threshold observed by Chamorro *et al.*[47] at which the mean wake flow becomes independent of Reynolds number. In addition, it is well established that most of the far wake characteristics are dependent on the turbine thrust coefficient.[4] The miniature turbine used in the current study is specifically designed to achieve a thrust coefficient close to the utility-scale turbines, which makes it possible to extend the findings of this study to the utility-scale turbines.

To characterize the incoming turbulent boundary layer, a combination of the 2D2C PIV system described earlier and a laser Doppler velocimetry (LDV) system is used. The LDV system used in the study is previously described by Dar *et al.*[18] A combination of the two techniques is employed for two reasons: the PIV field-of-view is not high enough to capture the boundary layer height, whereas for the LDV system, measurements near the ground cannot be captured due to the blockage of one of the laser beams close to the ground. Measurements are taken 20 m downstream of the test section inlet, where PIV measurements for different pressure gradient cases are taken. A comparison of the normalized averaged streamwise velocity U/U_h, where U_h is the hub height velocity, the streamwise turbulence intensity ($I_u = \sigma_u/U_h$, where σ_u is the standard deviation of the horizontal velocity), and the normalized averaged vertical momentum flux between the PIV and LDV is shown in Fig. 2. A good degree of agreement is observed in the overlapping region of the two measurement techniques for the normalized averaged streamwise velocity, streamwise turbulence intensity, and the normalized averaged vertical momentum flux. From the LDV measurements, the free stream velocity U_∞ is 9.7 m s^{-1}, where by using the criteria of $\delta = 0.99U_\infty$ the boundary layer height is estimated to be around 58.5 cm. This shows that the boundary layer height is almost twice compared to the height of the tallest ramp. A logarithmic profile is fitted to the PIV data in the surface layer to obtain the aerodynamic surface roughness z_0 and the friction velocity u_*. The logarithmic fit and measured velocity profile are shown in Fig. 2(d), where a friction velocity u_* value of 0.386 m s^{-1} and aerodynamic surface roughness z_0 of 0.1 mm are obtained.

B. Results

This section deals with the results from the PIV experiments. We first show the differences in the base flow (flow without the turbine) caused by the increase in the inclination of the ramps, for both the FPG and APG cases. For the turbine, we first show how the power coefficient is affected by the change in the pressure gradient and follow it up with a comprehensive wake flow analysis. For the mean flow, we define U as the time-averaged streamwise velocity, which is defined as $U = \sqrt{U_x^2 + U_z^2}$, where U_x and U_z are horizontal and vertical velocity components, respectively.

1. Base flow contours

We first characterize the base flow under different imposed pressure gradient situations. Figure 3 shows contours of the normalized averaged streamwise velocity along with flow streamlines for different

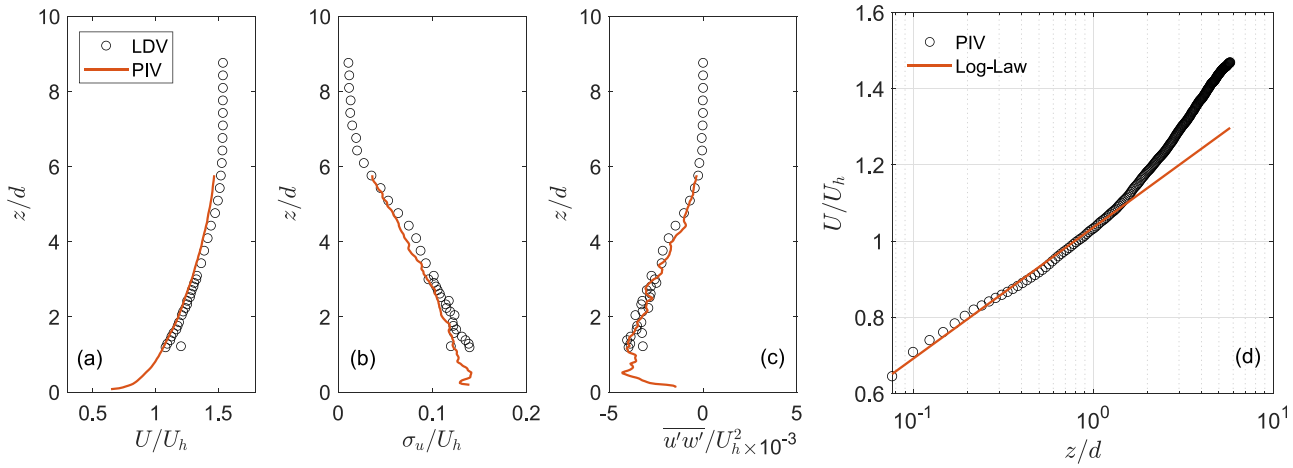

FIG. 2. Comparison of the (a) normalized averaged streamwise velocity, (b) streamwise turbulence intensity, and (c) normalized averaged vertical momentum flux obtained from PIV and LDV. (d) Normalized averaged streamwise velocity obtained in semi-logarithmic coordinates with the logarithmic fit in the brown line.

pressure gradients. Here, $(x, z) = (0, 0)$ represents the prospective turbine hub position. For ZPG, the streamwise velocity appears to be constant in the streamwise direction with a vertical shear, and the flow streamlines are parallel to the ground. Flow acceleration and deceleration is observed in FPG and APG cases, respectively. In FPG cases, the flow roughly follows the ramp angle at smaller ramp angles, whereas for higher ramp angles, the streamlines tend somewhat into the surface of the ramp, following an angle less than ramp angle. In high inclination APG cases, the flow appears to move away from the ramp surface, rather than following the ramp slope. No flow separation is observed in any of the modeled cases. As a more quantitative comparison between different cases, we plot the normalized averaged streamwise velocity at the local hub height as a function of the horizontal distance in Fig. 4. It can be readily seen that for the captured field-of-view, the flow speed-up and deceleration induced by the ramps is linear in all cases, whereas for ZPG the velocity is constant throughout the horizontal distance captured in this study. A flow speed-up of 1.33 with respect to the streamwise velocity at the hub height of the prospective turbine is observed for the highest FPG cases, whereas a deceleration to a value of 0.47 is seen for the highest APG case at $x/d = 7$. This translates to a flow speed-up of 4.7% per rotor diameter for the highest FPG case and a flow deceleration of 7.5% per rotor diameter for the highest APG case at a fixed local height above the surface with respect to the streamwise velocity at the prospective turbine location.

In the study by Shamsoddin and Porté-Agel,[32] the imposed pressure gradient is present only in the far wake, and exhibits a non-linear trend in the horizontal direction. The maximum speed-up and deceleration is about 1.55% and 0.67% per rotor diameter for the FPG and APG cases, respectively. For Dar and Porté-Agel,[44] adverse pressure gradients are induced by the escarpments with high pressure gradients in the near wake, which diminish in the far wake with a non-linear trend. In the study by Cai *et al.*,[34] the turbine is located at the edge of a ramp, where the base flow is initially affected by the curvature of the ramp edge. The flow speed-up in the highest FPG case is around 1.67% per rotor diameter and its deceleration is approximately 1.45% per rotor diameter in the highest APG case. Therefore, in the current study, we have created stronger pressure gradients than the ones tested before in the context of wind energy. Another key difference from previous studies is that the flow all the way from the turbine induction region through to its far wake is exposed to an approximately constant pressure gradient.

Figure 5 shows the contours of the horizontal turbulence intensity $I_x = \sigma_{U_x}/U_h$ for different pressure gradient situations. For the ZPG case, high turbulence intensity near the ground due to high flow shear is observed, which is approximately constant in the horizontal direction. The change in the ramp inclination has a significant influence on the mean flow shear, which results in the change in the turbulence intensity. For FPG cases, as the flow speeds up over the ramp, the mean flow shear near the ground decreases, which results in a decrease in the horizontal turbulence intensity with the increase in the horizontal distance. For the APG cases, on the other hand, as the flow moves away from the surface (shown previously using streamlines), the mean flow shear increases with an increase in the horizontal distance and ramp inclination, thereby resulting in an increase in turbulence intensity. The pressure gradient imposed by the terrain is characterized by the streamwise velocity gradient $((-1/\rho)\partial p/\partial x \approx U_b dU_b/dx)$,[31,32,44] where $dU_b/dx = 0$ corresponds to ZPG, $dU_b/dx > 0$ corresponds to FPG, and $dU_b/dx < 0$ corresponds to APG.

2. Power performance

Several studies have shown that terrain can have a significant influence on the power production of a wind turbine sited on it. Cai *et al.*[34] showed that the pressure gradient induced change in velocity can lead to a difference in the turbine power production compared to that in a flat terrain. More recently, Troldborg *et al.*[13] showed that the non-homogeneity of the base flow can affect the power coefficient of a wind turbine in a complex terrain compared to a reference power curve obtained in the flat terrain. In this work, we are interested in understanding the variation of the power coefficient of a turbine under a systematic change in the imposed pressure gradient.

Figure 6 shows the variation of the power coefficient as a function of normalized imposed pressure gradient at the turbine position. The

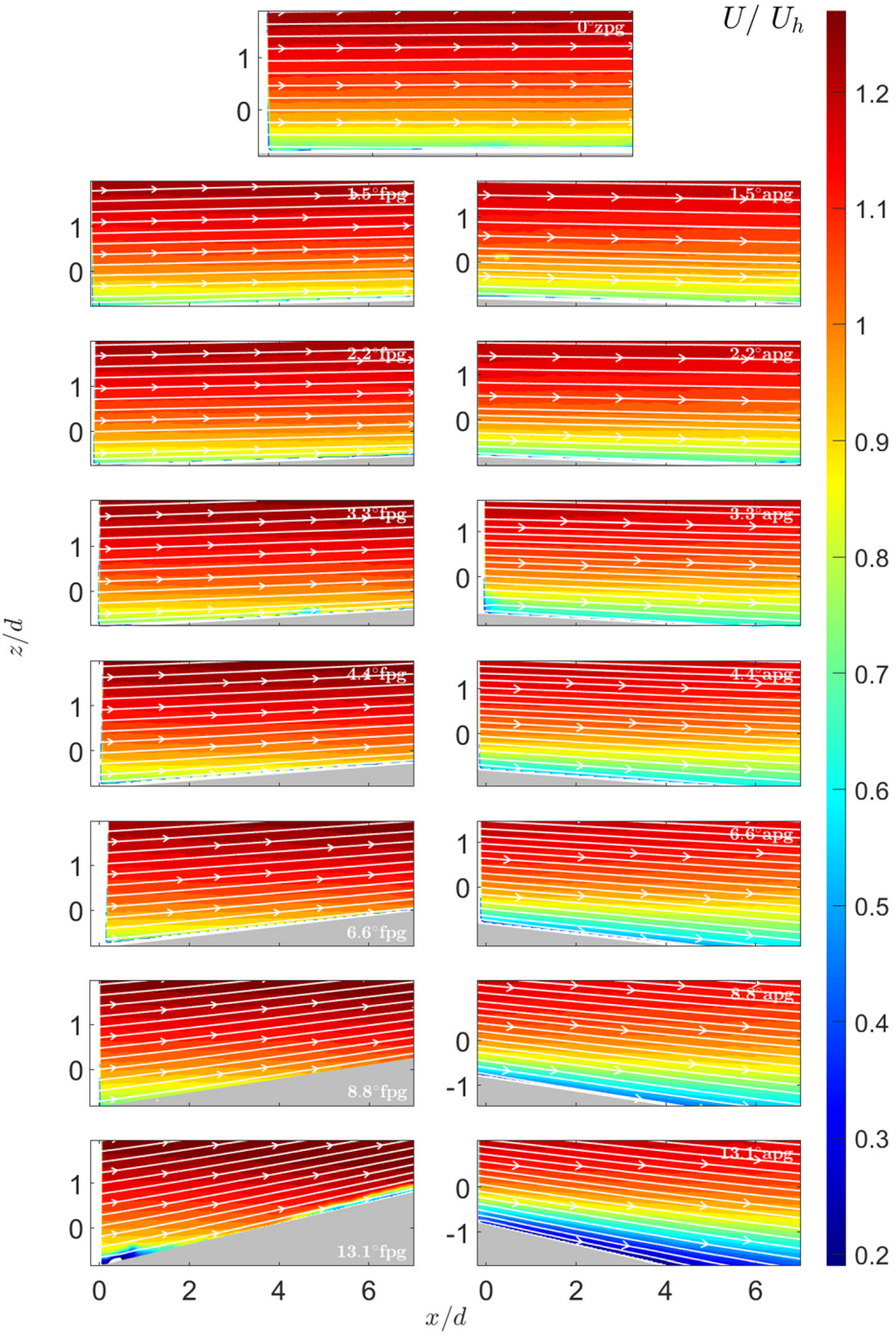

FIG. 3. Contours of the normalized averaged streamwise velocity in the base flow for different pressure gradient conditions. Mean flow streamlines are overlaid on the contours.

pressure gradient is characterized via the streamwise velocity gradient along the wake trajectory, which will be explained later in Sec. II B 3. The miniature turbine is always operated at an optimal tip speed ratio for a certain pressure gradient situation. For the ZPG case, a value of 0.347 is observed, which is similar to the one reported by Dar *et al.*[18] for the same turbine. This indicates that the power coefficient for the model wind turbine used in the study is insensitive to the turbulence intensity of the incoming flow, as the power curve in the study by Dar *et al.*[18] was measured at an incoming turbulence intensity of around 7%.

A general trend is observed, which shows that the power coefficient decreases with the increase in the adverse pressure gradient,

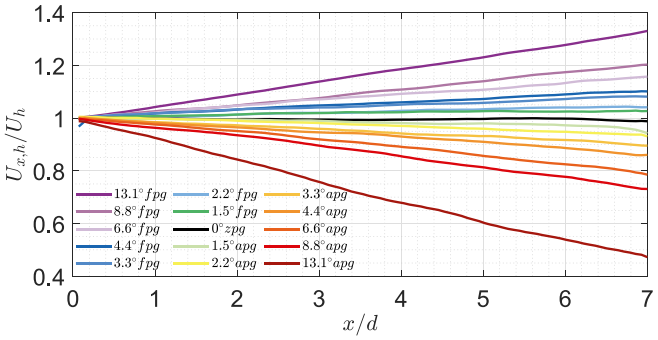

FIG. 4. Normalized averaged streamwise velocity at the local hub height above the ramp as a function of horizontal distance for different pressure gradient cases.

whereas it shows an increase with the increase in the favorable pressure gradient. The decrease in the power coefficient with the increase in the adverse pressure gradient is observed to be much stronger compared to the increase in the power coefficient with the increase in favorable pressure gradient. Quantitatively, C_P decreases by approximately 9.7% in the highest APG case compared to a 6.7% increase in the highest FPG case. However, the magnitude of the pressure gradient in the highest FPG case is twice that in the highest APG case. This indicates that an APG can have more severe consequences for a turbine power coefficient than the benefits obtained in a FPG situation. This can be particularly important for turbines sited on or around hillsides, where depending on the wind direction, a turbine will be operating in a favorable or adverse pressure gradient situation. Apart from the general trend, some anomalies are observed (e.g., 3.3° apg case), which could be related to the uncertainties in the power measurements, as discussed by Bastankhah and Porté-Agel.[39]

3. Wake flow contours

The effect of the pressure gradient on the turbine wake development is quantified in this section. Figure 7 shows the contours of the normalized averaged streamwise velocity in the turbine wake, along with the in-plane streamlines. For the FPG cases, the normalized averaged streamwise velocity shows an increase in magnitude compared to the ZPG case with the increase in the favorable pressure gradient, whereas for the APG cases, it decreases with the increase in the adverse pressure gradient. In addition, Fig. 8 shows the contours of the normalized averaged vertical velocity in the turbine wake. For the ZPG case, the normalized averaged vertical velocity is the smallest among all the cases. For the pressure gradient cases, the normalized averaged vertical velocity induced by the inclination of the ramp affects the vertical velocity in the wake flow. For FPG cases, the vertical velocity is mostly positive where an increase in magnitude with the increase in the ramp angle is observed. For the APG cases, a small region of positive vertical velocity is observed close to the turbine, whereas it is mostly negative due to the downward inclination of the ramps. To isolate the effect of the turbine on the wake velocity, we compute the streamwise velocity deficit $\Delta U = U_b - U_w$, where U_b is the time-averaged base flow velocity and U_w is the time-averaged wake flow velocity. Figure 9 shows the contours of the normalized averaged streamwise velocity deficit for different pressure gradient situations. Consistent with the previous studies,[28,32,34] the streamwise velocity deficit is observed to decrease with the increase in the FPG and increase with the increase in APG. This is attributed to the fact that a favorable pressure gradient enhances the wake recovery, whereas an adverse pressure gradient slows it down.

Looking at the wake trajectory, which is identified as the vertical position of the maximum streamwise velocity deficit at each horizontal position, it is observed that the wake does not follow the terrain for higher inclination angles. For the FPG cases, the wake shows a downward trajectory and becomes increasingly attached to the surface with the increase in the FPG, whereas for the APG cases, it moves away from the surface. It is shown that, to a good approximation, the wake trajectory follows the base flow streamlines—rather than traveling horizontally, or following a line of constant height above the surface of the hill. For the sake of brevity, the figure is shown in the Appendix. This is consistent with the findings of Liu *et al.*,[23] who showed that for several two- and three-dimensional hills, the wake follows the flow streamline originating from the turbine hub position. As a turbine wake is advected downstream by the surrounding base flow, it stands to reason that its trajectory is similar to the trajectory of the base flow. Therefore, subsequently, the base flow characteristics along the wake trajectory will be used to quantify the imposed pressure gradient and for wake modeling. In practical situations, where the wake trajectory can be an unknown quantity, the base flow streamline can be used as a proxy.

Figure 10 shows the contours of the horizontal turbulence intensity. A peak in turbulence intensity at the upper interface between the wake and the outer base flow is observed, which is commonly attributed to the high shear between the outer base flow and the low velocity wake flow. The magnitude of the turbulence intensity in the peak is observed to be dependent on the imposed pressure gradient. The horizontal turbulence intensity is observed to increase in peak magnitude with the increase in FPG, and decrease with the increase in APG. This may be related to the fact that a fixed hub height mean velocity is used to normalize the standard deviation of the velocity. If an alternate normalization is used, where the standard deviation is normalized with the base flow velocity along the wake trajectory, the FPG cases still show a higher peak in I_x close to the turbine. However, in the far wake, the APG cases show a higher peak (for the sake of brevity, the figure is not shown). This is understandable, as the APG slows down the wake recovery, thereby resulting in higher shear in the far wake compared to the FPG cases. As the wake does not follow the ramp, the turbulence intensity peak also moves into or away from the ramp for the FPG and APG cases, respectively.

4. Pressure gradient and turbulence intensity along wake trajectory

In Sec. II B 1, we quantified the flow speed up along the hub height over the ramps, which is useful and relevant from a resource assessment perspective prior to turbine placement. However, as seen in the previous section, the wake does not follow the ramp inclination, especially at high inclination angles. Therefore, here we quantify the velocity and associated pressure gradient along the wake trajectory. Figure 11 shows the normalized averaged streamwise velocity and the normalized pressure gradient along the wake trajectory. The flow speed up in the FPG cases is observed to be comparatively similar to

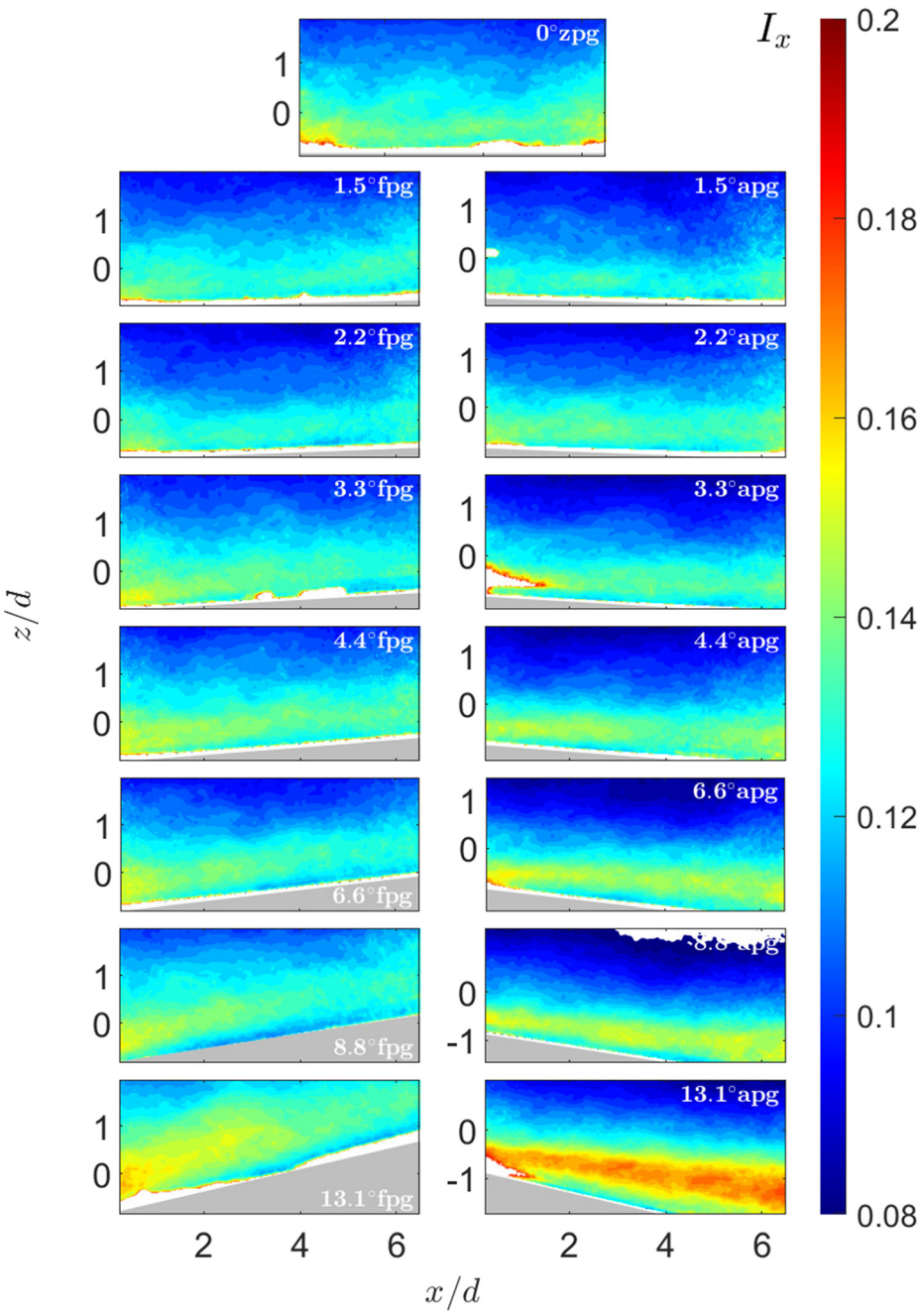

FIG. 5. Contours of the horizontal streamwise turbulence intensity in the base flow for different pressure gradient conditions.

that obtained along the hub height over the local surface. This is due to the fact that the downward trajectory of the wake is somewhat limited by the presence of a solid surface in the FPG cases. In the APG cases, on the other hand, the flow deceleration along the wake trajectory is comparatively less than that observed following the hub height over the local surface. This is attributed to the fact that, in APG cases, the wake trajectory is away from the surface into high velocity flow compared to that near the surface. The difference in the flow deceleration along the wake trajectory compared to flow deceleration along the local hub height is greatest for the two steepest APG cases. Somewhat surprisingly, the case with 13.1° inclination angle shows weaker wake deceleration at $x/d > 4$ than does the 8.8° case. This is explained by the fact that the wake trajectory moves away from the surface of the hill most strongly in the 13.1° case. Over all the cases, the maximum flow speed-up along the wake trajectory is 4.3% per rotor diameter (compared to 4.7%/d along the local hub height),

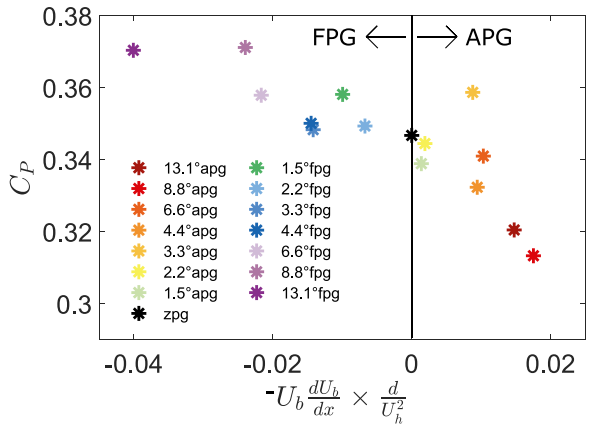

FIG. 6. Wind turbine power coefficient as a function of the normalized imposed pressure gradient.

whereas the maximum flow deceleration along the wake trajectory is 2% per rotor diameter (compared to 7.5%/d along the local hub height). The deceleration of 2% per rotor diameter is still higher than those reported in previous studies.[32,34]

Figure 11 (right) shows the trends in the imposed normalized pressure gradient for all ramp angles. The pressure gradients observed are approximately constant for most of the cases, except the extreme FPG case, where it increases with the increase in the distance. In addition, the magnitude of the pressure gradient in the maximum FPG case is more than twice the value in the maximum APG case. In the rest of this section, we will quantify some important wake characteristics as a function of the pressure gradient along the wake trajectory.

It is well known that the wake characteristics of a turbine depend on the base flow turbulence intensity. Figure 12 shows the rotor averaged turbulence intensity along the wake trajectory for all the cases. It can be seen that for most of the cases, the turbulence intensity lies within a close range of 0.12–0.14, and no systematic trend between the rotor averaged turbulence intensity and ramp angle is observed. Therefore, it can be concluded that within the limits of experimental setup, turbulence intensity has a minimal effect on the wake of the wind turbine, and the pressure gradient is the dominating factor responsible for the systematic differences observed in the turbine wake.

5. Wake center recovery

Recovery of the wake center velocity deficit is an important wake characteristic, quantified by the evolution of the maximum velocity deficit with distance from the turbine. Figure 13 shows the maximum normalized streamwise velocity deficit for different pressure gradients. The maximum normalized streamwise velocity deficit in the turbine wake is observed to be affected by the pressure gradient, with the highest APG case showing the largest deficit and the highest FPG case showing the smallest one. In addition, the maximum deficit near the turbine is also shifted higher (lower) in the APG (FPG) cases compared to that in the ZPG case. This is associated with the effect of the pressure gradient on the turbine induction, which affects the maximum velocity deficit in the near wake. A similar observation was made by Dar and Porté-Agel,[17] who found that the maximum velocity deficit in the proximity of the turbine is affected by the adverse pressure gradient imposed by an escarpment. This is due to the fact that in addition to the turbine thrust, the pressure gradient also contributes to the streamwise momentum in the turbine wake.[31,32] Depending on the sign of the pressure gradient (favorable or adverse), it either subtracts or adds to the contribution from the turbine thrust. As an adverse pressure gradient slows the wake recovery, it adds to the maximum velocity deficit contribution from the turbine thrust, whereas the favorable pressure gradient subtracts from it.

The effect of pressure gradient can be observed even more clearly in Fig. 13 (right), which subtracts the maximum streamwise velocity deficit in the ZPG case from all the cases. All the APG cases show a positive difference from the ZPG cases, whereas all the FPG cases show a negative one. Interestingly, the difference shows a variation near the turbine, while, in the far wake, it reaches a nearly constant value, which depends on the pressure gradient. The variation in the difference with respect to the ZPG velocity deficit maximum close to the turbine can be partly associated with the difference in the near wake length in different cases. The near wake length is shorter (longer) for the FPG (APG) cases compared to that for the ZPG case. A shorter near wake length indicates an earlier re-energization of the wake center velocity deficit compared to that in the ZPG case, which explains why the difference between the FPG and ZPG cases is more pronounced than that between the APG and ZPG cases. The relation between the near wake length and the imposed pressure gradient will be discussed in detail in the remainder of this section.

6. Near wake length

The near wake of a turbine is characterized as the region close to the turbine where the flow has a "memory" of the turbine geometry. It is a region of complex flow marked by the tip and hub vortices, rotation of the wake, and wake of the turbine nacelle. A simplified approach is to assume a gradual transition from a top-hot velocity profile at the turbine position to a Gaussian velocity profile at the end of the near wake. The length of the near wake, defined as the downstream distance until which the wake flow has a memory of turbine geometry, has been shown to depend on many factors such as the incoming turbulence intensity, the turbine thrust coefficient, and the turbine tip speed ratio.[4] Here, we are interested in understanding the dependence of the near wake length on the pressure gradient imposed by the terrain. This is motivated by the fact that the end of the near wake region marks the onset of the far wake, which is of most interest for the wind energy community, especially from the perspective of wind resource assessment, layout optimization and analytical wake modeling.

Several methods are used in the wind energy community to characterize the near wake length. Of these, the most commonly used ones are the downstream distance at which the streamwise velocity deficit profiles become Gaussian,[4] and the downstream distance at which the maximum streamwise velocity deficit becomes equal to the theoretically predicted maximum.[48–50] In the following, we will compare the near wake length obtained from both these criteria and comment on their differences. For the first criterion, which is based on the downstream distance from the turbine at which the streamwise velocity deficit profile becomes Gaussian, we perform a Gaussian fitting on the vertical profiles of the streamwise velocity deficit at each horizontal

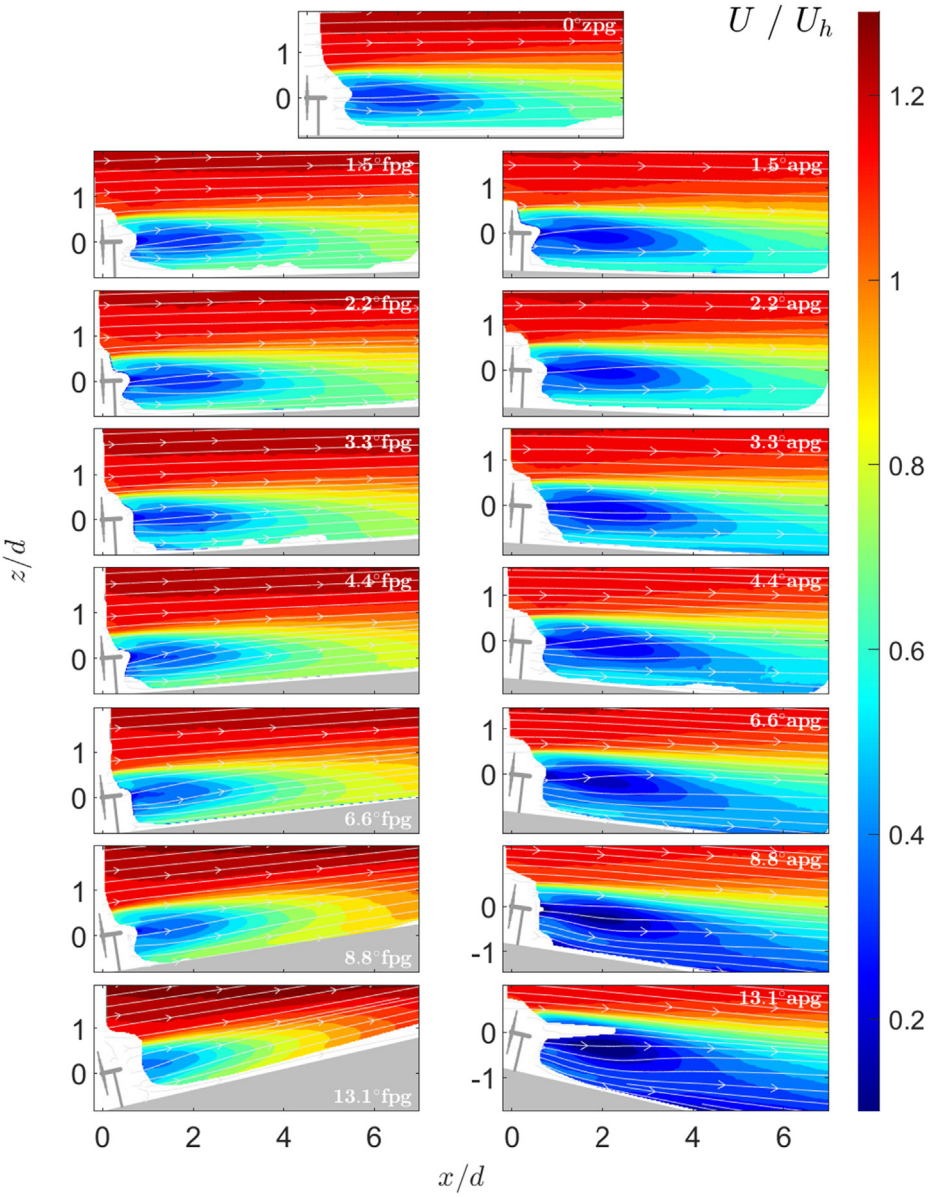

FIG. 7. Contours of the normalized averaged streamwise velocity in the wake flow for different pressure gradient conditions. Mean flow streamlines are overlaid on the contours.

position. The goodness of the fit, identified by the coefficient of determination ($R^2 > 0.985$), is used to identify the onset of the far wake, and the distance from the turbine at which it is obtained is classified as the near wake length. For the second criterion, we employ the definition of the near wake velocity under pressure gradient using one-dimensional momentum theory given by Dar and Porté-Agel.[44] The near wake velocity under the pressure gradient is defined as: $U_{nw} = \sqrt{U_{nb}^2 - U_h^2 C_T}$, where U_{nw} is the near wake velocity, U_{nb} is the base flow velocity in the near wake, U_h is the hub height velocity and C_T is the turbine thrust coefficient. In the context of Dar and Porté-Agel,[44] U_{nb} was fixed at a location near the turbine where the wake flow pressure and base flow pressure equalize—to ensure that the defined equation yields a real value, which resulted in a constant near wake velocity. Here, we generalize this approach by keeping U_{nb} variable with the downstream distance in the near wake. This is done to account for the variation in the near wake velocity deficit maxima due to the pressure gradient in the streamwise direction. Given that the above-defined equation yields real values for all cases, it is possible to evaluate the feasibility of this approach. For analytical modeling in Sec. III, the same approach will be adopted and validated to account for the effect of pressure gradient in the near wake of the turbine.

Figure 14(a) shows the normalized near wake length obtained from the two criteria defined above as a function of the imposed pressure gradient. Overall, both criteria show similar trend between the imposed pressure gradient and the normalized near wake length. In general, the near wake length shortens with the increase in the

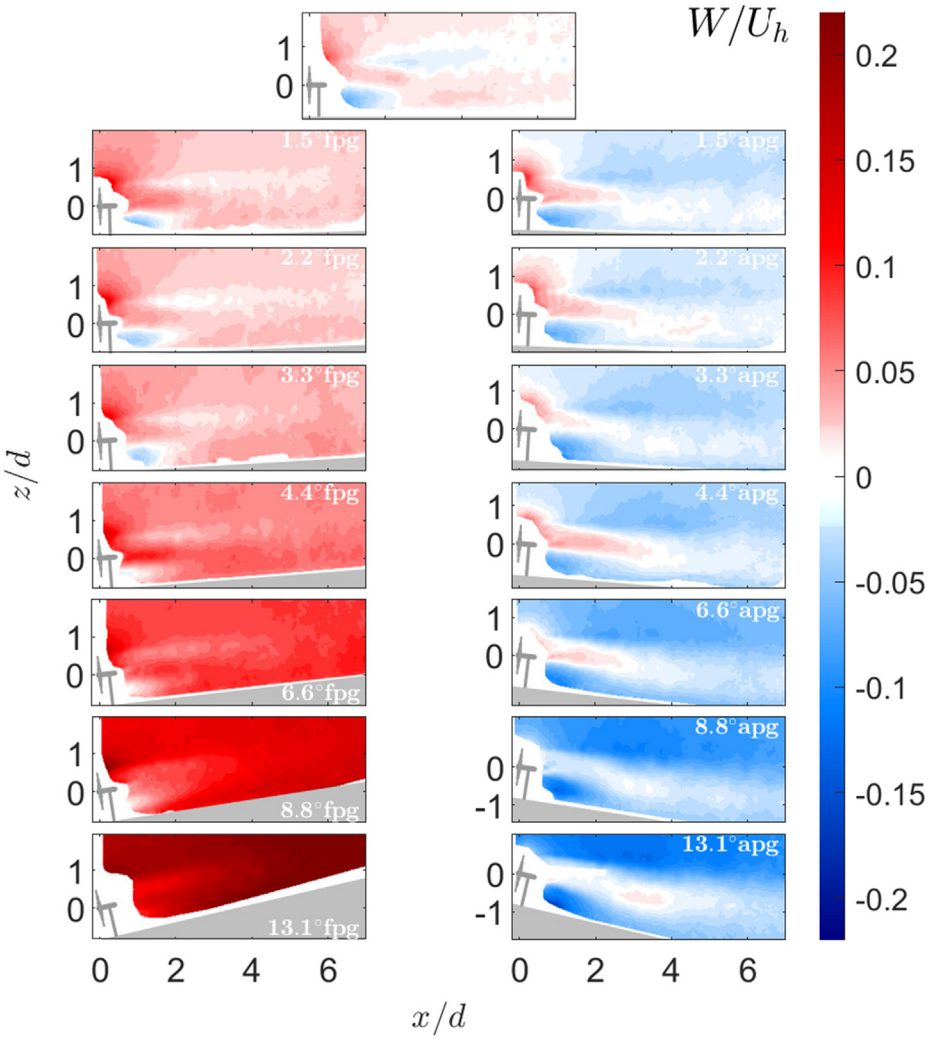

FIG. 8. Contours of the normalized averaged vertical velocity in the wake flow for different pressure gradient conditions.

favorable pressure gradient, and lengthens with the increase in the adverse pressure gradient compared to that in the ZPG case. As FPGs results in base flow acceleration, it leads to an acceleration in the growth of the shear layer surrounding the rotor periphery, thereby bringing higher energy flow into the wake center at an earlier downstream position compared to the ZPG case, which explains the shorter near wake length. The opposite can be said about the adverse pressure gradient, which slows down the growth of the shear layer between the wake and base flow compared to the ZPG case. A bivariate correlation coefficient of 0.89 is measured between the imposed pressure gradient and the normalized near wake length which indicates a strong positive statistically significant correlation.

Although both criteria for near wake length show similar trend, there appears to be an offset between the near wake length values obtained from these criteria. This offset is in the range of 0.9–1.3 rotor diameters for different pressure gradient cases. In the following we attempt to provide a physical explanation for this offset. As noted in previous studies,[17,18,49] the miniature wind turbine used in the study usually shows a higher maximum streamwise velocity deficit in the near wake than what is predicted by the simplified one-dimensional momentum theory. This can be attributed, among other factors, to the wake of the turbine nacelle. As the one-dimensional momentum theory is designed for actuator disks with no nacelle, it does not account for the drag of the nacelle in the near wake of the turbine. It is commonly assumed that as the shear layer grows enough to reach the wake center, the wake deficit profiles become Gaussian. For actuator disks without any nacelle, the maximum velocity deficit at this position will be the same as that predicted by the one-dimensional momentum theory. However, in the current scenario, the maximum velocity deficit at this position is higher than the one obtained from the one-dimensional momentum theory, as the wake still has to recover the deficit caused by the nacelle. Therefore, the maximum velocity deficit at the position where the profiles first show a Gaussian shape is higher than that predicted by the one-dimensional momentum theory. It can be assumed that the offset between the values of near wake length obtained from the two criteria is accounted for by the extra distance it

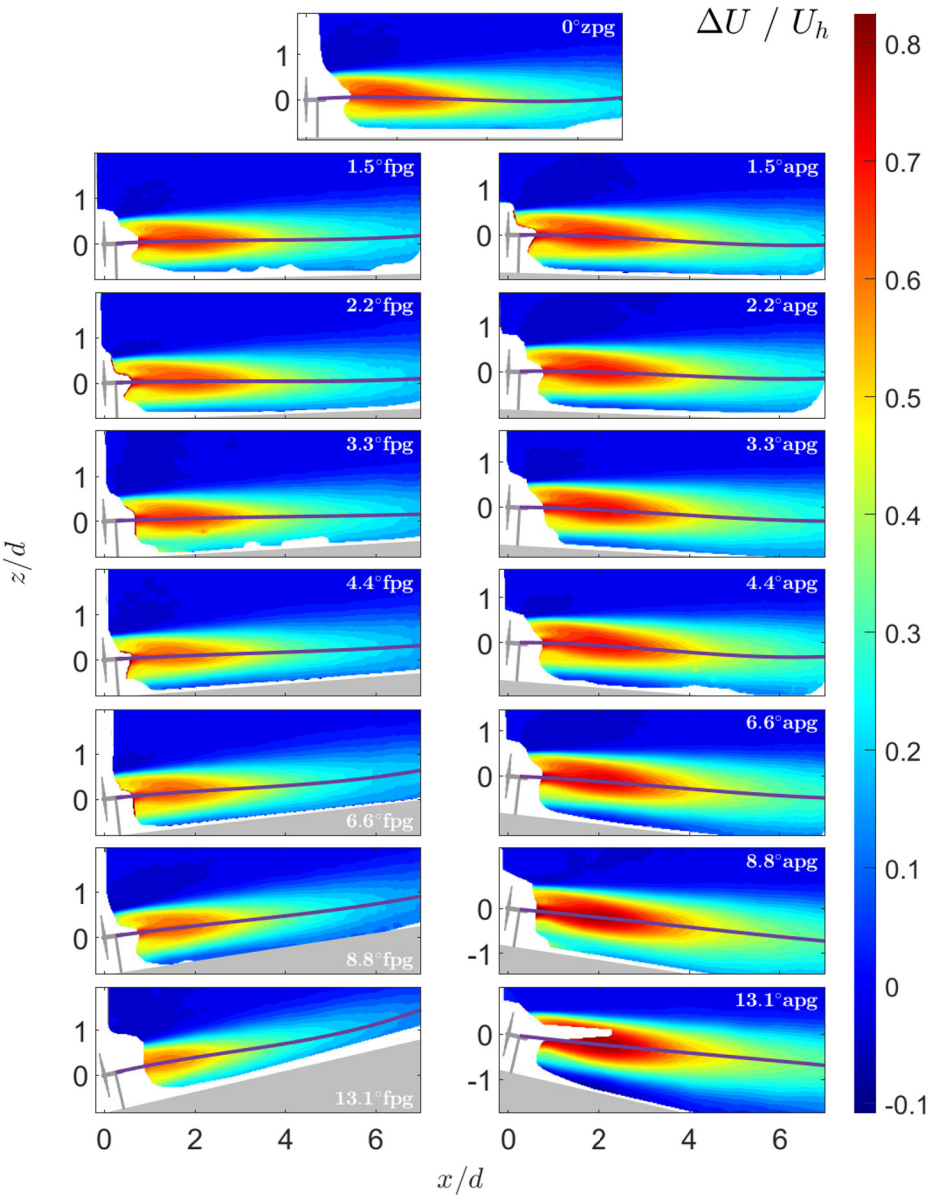

FIG. 9. Contours of the normalized averaged streamwise velocity deficit in the wake flow for different pressure gradient conditions. The solid line represents the wake trajectory.

takes to recover the maximum velocity deficit contributed by the turbine nacelle. The fact that the offset lies within a close range for all the cases supports this hypothesis.

It is well agreed upon in the literature that near wake length depends on the incoming flow turbulence intensity, where higher turbulence leads to a shorter near wake length.[51] To ensure that the correlations observed here between pressure gradient and near wake length, are not simply a result of correlated turbulence intensity, we correlate normalized near wake length as a function of the rotor averaged horizontal turbulence intensity in the base flow in Fig. 14(b). It can be seen that the rotor averaged turbulence intensity lies in a relatively tight range of 0.125–0.155 between cases, and that the spread of the data perpendicular to its linear regression line is large relative to its span parallel to the line. The bivariate correlation coefficient in the data are −0.61, indicating a statistically insignificant correlation between near wake length and rotor averaged turbulence intensity.

7. Wake growth rate

As the wind turbine wake moves downstream, it expands radially in the cross-stream direction. This is due to the growth of the shear layer around the rotor periphery and related mixing of the wake with the outer base flow. The rate at which wake expands in the cross-stream direction with the increase in the streamwise distance is known as the wake growth rate. In the far wake, it is well known that the wake grows linearly in flat,[4] as well as complex terrain.[17,18] To quantify the

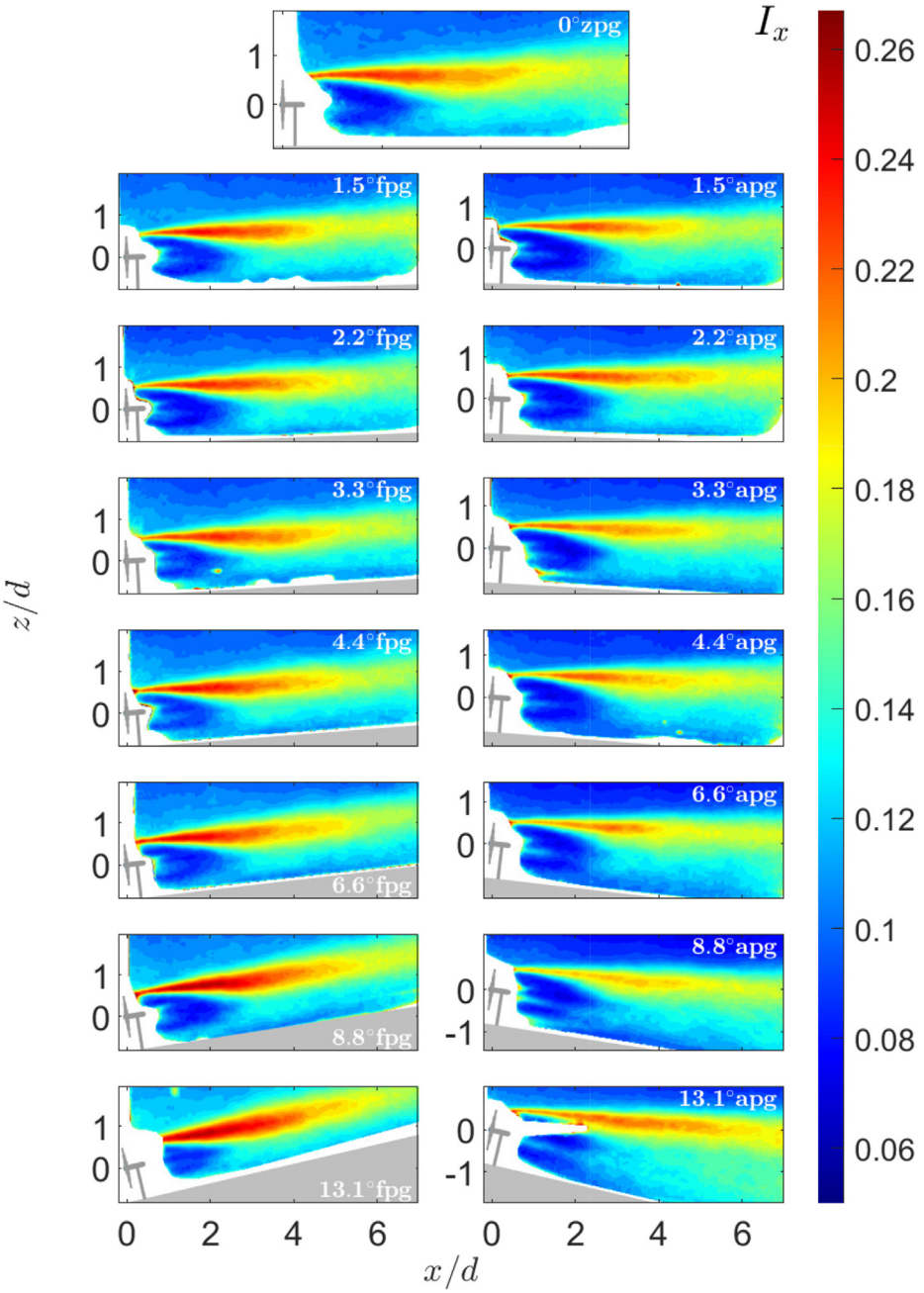

FIG. 10. Contours of the horizontal turbulence intensity in the wake flow for different pressure gradient conditions.

wake growth rate, the wake width at any downstream distance needs to be quantified. One approach is to characterize the wake width as the standard deviation of a Gaussian fit to the cross-stream profile (either lateral or vertical). The slope at which the standard deviation grows with the increase in the streamwise distance identifies the wake growth rate. This is done according to the following relation: $\frac{\sigma_z}{d} = k\frac{x}{d} + \epsilon$, where σ_z is the wake width in the vertical direction, k is the wake growth rate, and ϵ is the initial wake width.

Here, we are interested in finding a systematic relation between the wake growth rate and the imposed pressure gradient. Figure 15(a) shows the wake growth rate as a function of the imposed pressure gradient. Once again, a clear difference between the FPG and APG cases can be observed, with the ZPG case lying in the middle. The wake growth rate is observed to decrease with the increase in the FPG and increase with the increase in the APG compared to that in the ZPG case. A strong positive (statistically significant) trend is measured

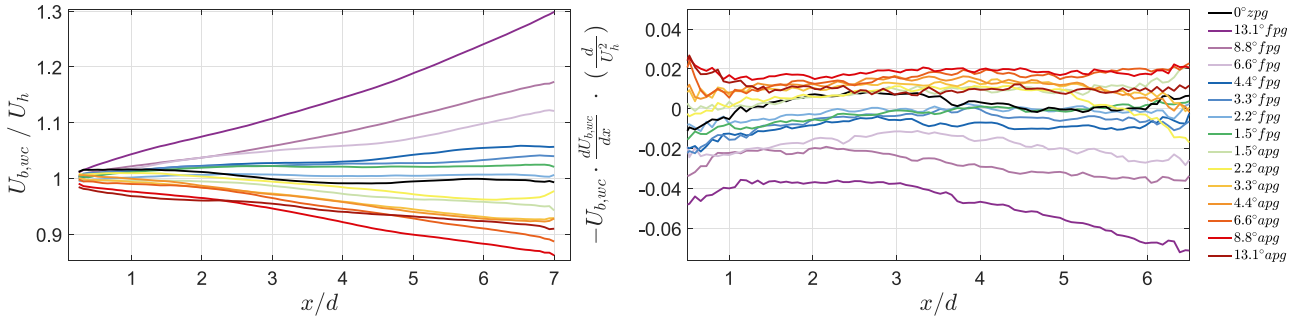

FIG. 11. Normalized averaged streamwise velocity (left) and normalized pressure gradient (right) in the base flow along the wake trajectory across different ramp angle cases.

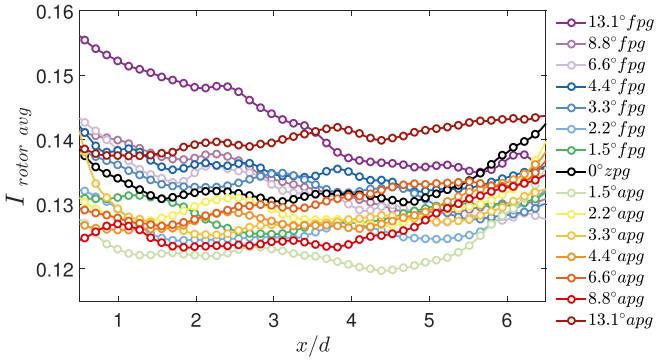

FIG. 12. Rotor averaged horizontal turbulence intensity along wake trajectory.

between the two parameters, with a bivariate correlation coefficient of 0.92. Moreover, there appears to be a linear relation between the imposed pressure gradient and the wake growth rate. This relation is given as $k = 0.311 \times PG + 0.053$, where PG is the non-dimensional imposed pressure gradient $(-U_b \frac{dU_b}{dx} \times \frac{d}{U_h^2})$. The wake growth rates are obtained based on the vertical profiles of the streamwise velocity deficit only, which could differ from a wake growth rate measure that takes into account the lateral wake width.

Similar to the near wake length, the wake growth rate is also known to be dependent on the ambient turbulence intensity.[4] We plot the estimated wake growth rates as a function of rotor averaged horizontal turbulence intensity in Fig. 15(b). A very wide spread in the wake growth rates is seen when plotted against turbulence intensity. Additionally, the wake growth rates are lower for higher turbulence intensity, which is opposite to what would be expected without the presence of any pressure gradient. It can therefore be said that the differences in the wake growth rates observed here can only be explained by the imposed pressure gradient.

III. ANALYTICAL MODELING

Analytical models provide a reasonably accurate and computationally cheap estimation of the wake velocity deficit behind a turbine. Such models are widely used in the wind energy community to estimate the effects of wakes on power available within a wind farm and facilitate testing multiple layouts and wind directions in a relatively short time. In the following, we provide an assessment of some common analytical modeling approaches available in the literature for wakes under pressure gradient.

A. Standard Gaussian model

One of the most popular analytical models used today is the Gaussian wake model proposed by Bastankhah and Porté-Agel.[39,49] This model is derived using mass and momentum conservation under an assumption of a zero pressure gradient and uses the self-similarity of the streamwise wake velocity deficit to produce the velocity deficit profiles. Despite the fact that the model is derived under an assumption of a ZPG, it is a fairly common practice in the wind energy community to use it in complex terrain with a pressure gradient. A

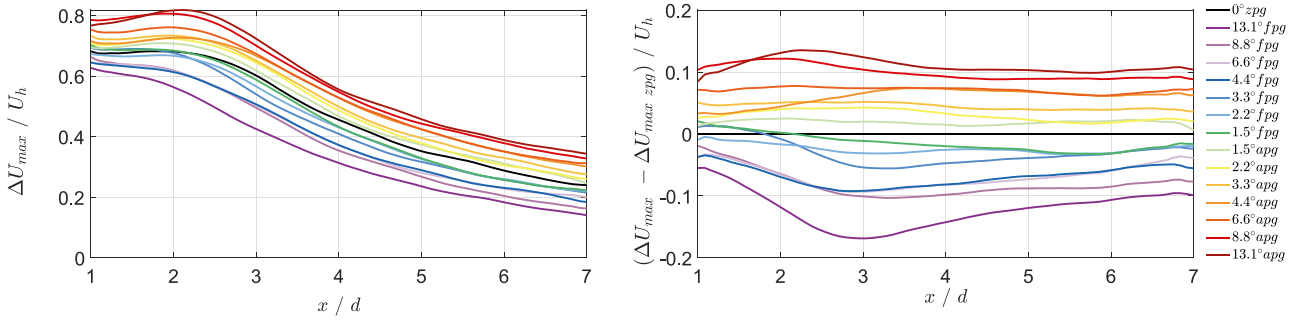

FIG. 13. Maximum normalized streamwise velocity deficit as a function of streamwise distance for different pressure gradient cases (left), and maximum normalized velocity deficit minus ZPG normalized velocity deficit for different pressure gradient cases (right).

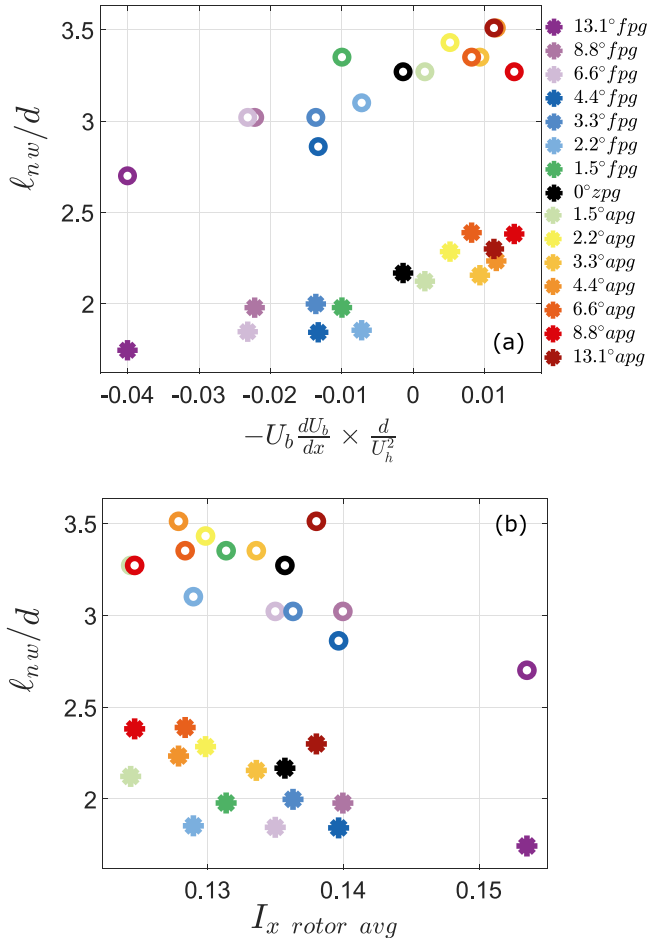

FIG. 14. Normalized near wake length as a function of imposed pressure gradient in the near wake (a), and as a function of rotor averaged turbulence intensity in the near wake (b). Circles denote the near wake length using the criteria of maximum theoretical streamwise velocity deficit and stars denote the near wake length using the criteria of a Gaussian streamwise velocity deficit profile.

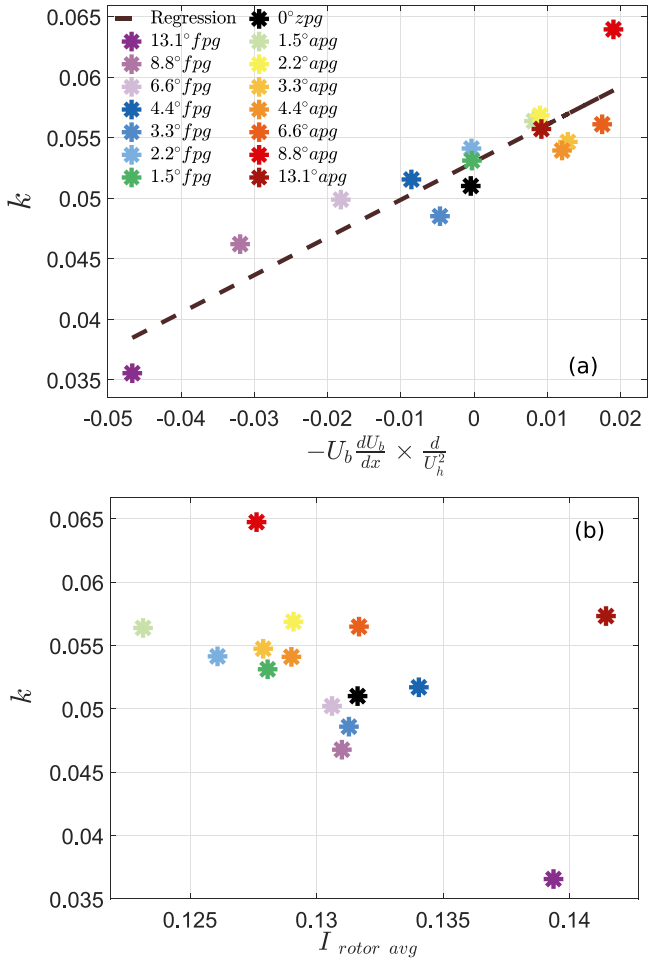

FIG. 15. Wake growth rate as a function of imposed pressure gradient (a), and as a function of rotor averaged turbulence intensity in the far wake (b). The dashed line shows a linear fit to the data.

common approach to implement the Gaussian model in complex terrain is to superpose the velocity deficit obtained from the model on a varying base flow velocity field. In other words, the reference base flow velocity in the Gaussian model is assumed to be a function of the streamwise distance rather than a fixed value. A few recent examples of such adaptation of the Gaussian model are given in Refs. 42, 43, 52, and 53.

In the current work, our objective is to assess the accuracy of this common approach across a range of imposed pressure gradient. We aim to find a threshold in terms of the flow speed-up or deceleration caused by the imposed pressure gradient up to which the simple approach of superposing the standard Gaussian model on varying base flow can yield reasonable results.

The streamwise wake velocity deficit in the far wake is given by

$$\frac{U_b - U_w}{U_b} = C(x)e^{-\left(\frac{r^2}{2\sigma(x)^2}\right)}, \tag{1}$$

where $C(x)$ is the maximum normalized streamwise velocity deficit, r is the radial distance from the wake center, and σ is the wake width. The maximum normalized streamwise velocity deficit $C(x)$ is obtained from streamwise momentum balance and written as a function of the turbine thrust coefficient C_T and the wake width σ in the far wake. Here, we use the formulation of the Gaussian model given by Bastankhah and Porté-Agel,[49]

$$C(x) = 1 - \sqrt{1 - \frac{\sigma_0^2 C_0(2 - C_0)}{\sigma(x)^2}}, \tag{2}$$

where σ_0 is the wake width at the start of the far wake taken from the experiments, C_0 is the maximum streamwise velocity deficit at the start of the far wake obtained from the one dimensional momentum theory ($C_0 = 1 - \sqrt{1 - C_T}$, where $C_T = 0.8$), and σ is the wake width in the far wake. The wake growth rate k needed to compute σ is obtained from the relation between the wake growth rate and base flow streamwise turbulence intensity, given as: $k = 0.3I$.[54]

Figure 16 shows the comparison of the maximum normalized averaged streamwise velocity deficit obtained from the experiments and from the model equation (2). The model prediction agrees well with the experimental data for the ZPG case. However, the difference between the experiments and the model increases with the increase in the pressure gradient. Figure 17 shows the comparison of the vertical profiles of the normalized averaged streamwise velocity deficit between the experiments and the model at several downstream positions. For smaller imposed pressure gradients, the streamwise velocity deficit profiles seem to show a reasonable agreement between the Gaussian model and the experiments. However, the error in both the maximum deficit and the wake width grows with increasing magnitude of the imposed pressure gradient for both favorable and adverse pressure gradients. Furthermore, the model predicts a slower wake recovery under favorable pressure gradients, and faster under adverse—opposite to the trend actually observed in the experiments. The superposition of the Gaussian model on varying base flow fails to capture the correct qualitative trend for wake velocity deficit under imposed pressure gradients. For the interested reader, this is explainable: take the case for example of favorable pressure gradients. As the base flow speeds up along the streamwise direction, the model subtracts the same ZPG wake velocity from a faster base flow, leading to a greater predicted deficit, and an apparent slowed wake recovery—contrary to what is experimentally observed.

It is of potential importance to the wind community to define a threshold condition above which it becomes inappropriate to use the superimposed Gaussian model. For the APG cases, the Gaussian model yields a reasonable result only up to a ramp inclination of 2.2°, which corresponds to a flow deceleration of ≈0.57% per rotor diameter along the wake trajectory. For the 3.3° APG case, which corresponds to a flow deceleration of ≈1% per rotor diameter along the wake trajectory, the model shows significant deviation from the experiments. For the FPG cases, on the other hand, an acceptable agreement between the Gaussian model and experiments is observed up to a ramp inclination of 3.3°, which also corresponds to a flow speed-up of ≈0.59% per rotor diameter along the wake trajectory. We have shown that the range of pressure gradient conditions over which the simplistic approach of superimposing the Gaussian model predicted deficit on a changing base flow works is relatively small. This indicates that special attention must be paid to the base flow acceleration before using the Gaussian model in complex terrain. In practical situations, where the wake trajectory is unknown, flow acceleration along the base flow streamlines can be used as an alternative, as discussed previously in Sec. II B 3.

B. Pressure gradient model

In this section, we investigate if an analytical model derived for the pressure gradient can provide a better prediction than the standard Gaussian model. For this purpose, we use the model initially derived by Shamsoddin and Porté-Agel[32] for the effect of an imposed pressure gradient on the far wake and further extended to account for an imposed pressure gradient in the near wake by Dar and Porté-Agel.[44] A brief summary of the model along with the procedure followed to obtain the velocity deficit profiles is given below. In addition, we complement the pressure gradient model with a theoretical relation for the estimation of the near wake length.

Similar to the standard Gaussian model, the far wake streamwise velocity deficit is self-similar and has a Gaussian shape function under the pressure gradient. Therefore, its functional form is also given by Eq. (1). The streamwise evolution of the maximum velocity deficit, wake width, and the onset of the far wake, however, are dependent on the imposed pressure gradient. The base flow velocity along the wake trajectory is used as an input for the model. The normalized maximum streamwise velocity deficit in the far wake is estimated using the following ordinary differential equation:

$$\frac{dC}{dx} = \frac{-1}{\left(\frac{U_b^4}{\Lambda_0^2}\right)(3C^2 - 2C^3)}\left[\frac{1}{4}\frac{dU_b^4}{dx}\frac{C^3}{\Lambda_0^2} + \left(C^3 - \frac{C^4}{2}\right)\frac{d}{dx}\left(\frac{U_b^4}{\Lambda_0^2}\right)\right], \tag{3}$$

where Λ_0 is the ratio of streamwise velocity deficit to wake width, which is known to be invariant to the pressure gradient.[29,32] This invariant ratio is defined as

$$\Lambda_0 = \frac{C_{zpg}U_{zpg}}{\sigma_{zpg}}, \tag{4}$$

where C_{zpg}, U_{zpg}, and σ_{zpg} are the maximum normalized velocity deficit, base flow velocity, and wake width under zero pressure gradient. The wake width under the pressure gradient is estimated using the invariant ratio and is given by

$$\sigma(x) = \frac{CU_b}{\Lambda_0}. \tag{5}$$

Equation (3) is valid in the turbine far wake, and it needs the near wake velocity deficit as a boundary condition. Dar and Porté-Agel[44] provided an analytical equation for the near wake velocity deficit under pressure gradient,

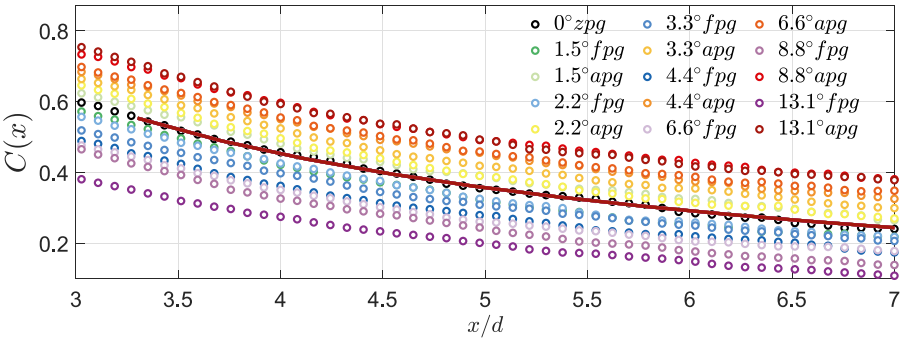

FIG. 16. Comparison of the normalized maximum streamwise velocity deficit $C(x)$ obtained from the Gaussian model (solid line) and the experiments (circles) for different imposed pressure gradients.

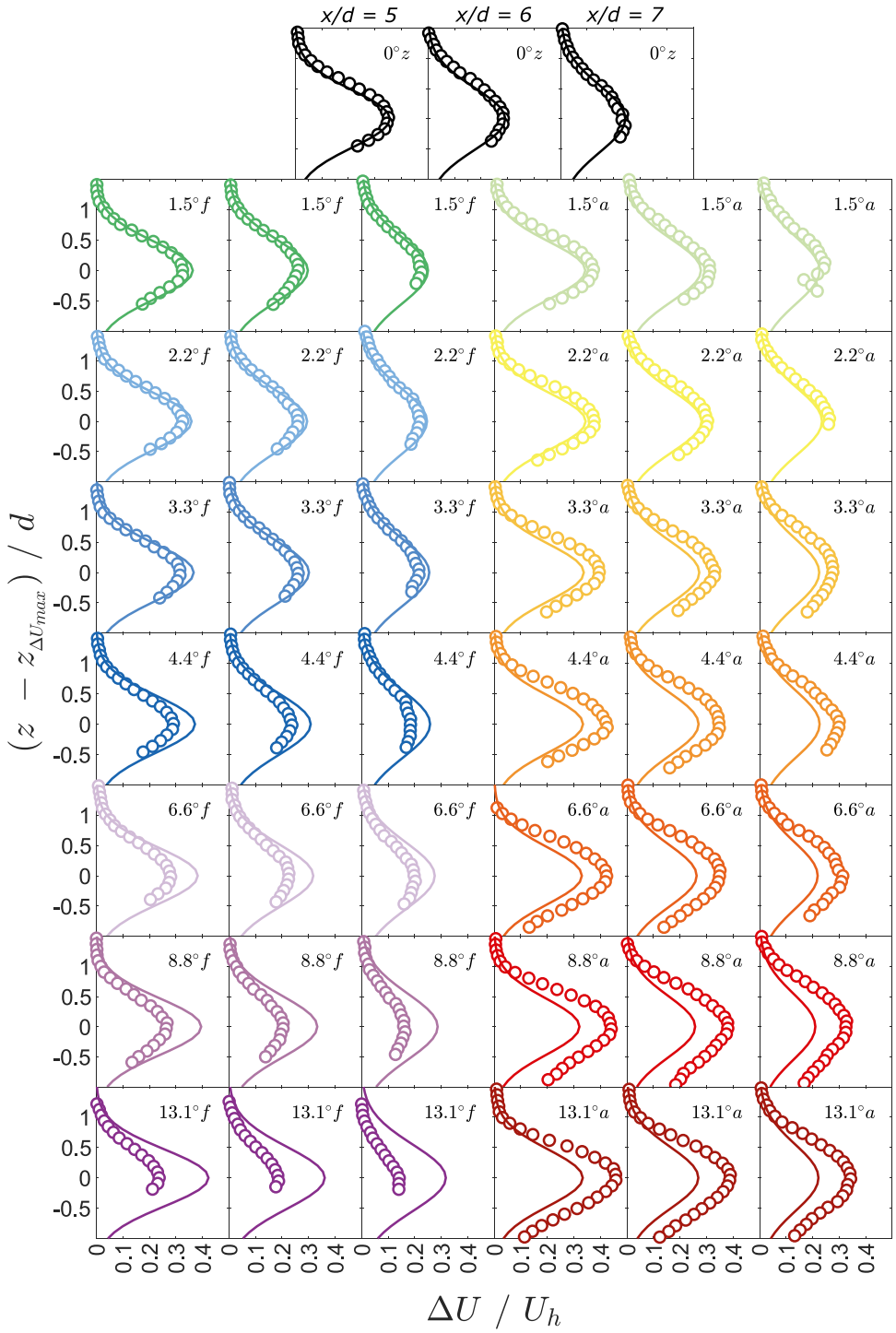

FIG. 17. Comparison of the vertical profiles of the normalized averaged streamwise velocity deficit between the experiments (circles) and the Gaussian model (solid line) at selected downstream positions.

$$C_{nw}(x) = 1 - \frac{U_{nw}(x)}{U_b(x)}, \tag{6}$$

where $C_{nw}(x)$ is the normalized maximum velocity deficit in the near wake and U_{nw} is the near wake velocity, which can be obtained as follows:

$$U_{nw}(x) = \sqrt{U_{nb}(x)^2 - U_h^2 C_T}, \tag{7}$$

where U_{nb} is the base flow velocity in the near wake. In the model validation of Dar and Porté-Agel,[44] the near wake velocity was assumed

to be a constant and obtained at the position where the base and wake flow pressure equalize. This distance was fixed at 1 rotor diameter downstream of the turbine. Here, we generalize this approach by keeping the near wake velocity variable. Contrary to Dar and Porté-Agel,[44] Eq. (7) yields real values throughout the near wake due to a linear speed-up/slow down of the base flow in the current study, enabling us to test this approach.

In addition to the analytical relations for near and far wake velocity deficit, an estimation of the near wake length is needed to switch the model from near to far wake solution. Currently, no analytical relations for the length of near wake under a pressure gradient exist. In the following, we derive a theoretical relation for near wake length under an imposed pressure gradient.

The near wake of a turbine is characterized by the growth of a shear layer behind the rotor periphery. This shear layer expands radially as the wake is advected downstream due to the mixing between the low energy wake flow and the high energy base flow outside the wake. Following Bastankhah and Porté-Agel,[49] the near wake length can be characterized as the distance downstream of the turbine where the shear layer width reaches the wake center, thus energizing the wake center. In their study, Bastankhah and Porté-Agel[49] generalized the model for the growth of a shear layer originally proposed by Lee and Chu[55] to account for the effects of turbulence intensity and velocity difference between the wake and outer flow on the development of a shear layer. However, their derivation was meant for the growth of a free shear layer under a zero pressure gradient. Here, we will further generalize their model for an arbitrary pressure gradient.

According to Bastankhah and Porté-Agel,[49] the variation of a free shear layer width can be expressed as

$$\frac{1}{U_\infty}\frac{ds}{dt} = \frac{U_s}{U_\infty}\frac{ds}{dx} = \alpha I + \beta\frac{U_e}{U_\infty}, \tag{8}$$

where U_∞ is a constant velocity of the flow outside the wake, s is the width of the shear layer, t is the time, U_s is the characteristic velocity of the shear layer defined as $0.5(U_\infty + U_{nw})$, U_e is the relative velocity in the shear layer given by $0.5(U_\infty - U_{nw})$; finally, α and β are model constants. Under the assumption of a zero pressure gradient, all the velocities in Eq. (8) are constant, which simplifies the model. For the development of a free shear layer under an imposed pressure gradient, Eq. (8) can be interpreted as a local relation and re-written as follows:

$$\frac{1}{U_b(x)}\frac{ds}{dt} = \frac{U_s(x)}{U_b(x)}\frac{ds}{dx} = \alpha I + \beta\frac{U_e(x)}{U_b(x)}, \tag{9}$$

where $U_b(x)$ is the local base flow velocity, $U_s(x)$ is the local shear layer characteristic velocity defined as $0.5(U_b(x) + U_{nw}(x))$, and $U_s(x)$ is the local relative velocity estimated by $0.5(U_b(x) - U_{nw}(x))$. The integral form of Eq. (9) can be written as follows:

$$\int_0^{\sigma_{nw}} ds = \int_0^{l_{nw}} \frac{U_b(x)}{U_s(x)}\left[\alpha I + \beta\frac{U_e(x)}{U_b(x)}\right]dx. \tag{10}$$

Inserting expressions for different velocities in the above equation yields:

$$\sigma_{nw} = (2\alpha I + \beta)\int_0^{l_{nw}} \frac{1}{1+\frac{U_{nw}(x)}{U_b(x)}}dx - \beta\int_0^{l_{nw}} \frac{1}{1+\frac{U_b(x)}{U_{nw}(x)}}dx. \tag{11}$$

Equation (11) is a general equation, which can be solved for any form of base flow $U_b(x)$ to estimate the near wake length. Here, we will solve Eq. (11) in the context of the current work. For this purpose, we assume the base flow to be linear and express it as $U_b(x) = (\gamma x + U_h)$, where γ is the flow speed-up factor, which will be positive for FPG and negative for APG. Inserting the functional form of $U_b(x)$ and $U_{nw}(x)$ in Eq. (11) yields

$$\sigma_{nw} = (2\alpha I + \beta)\int_0^{l_{nw}} \frac{1}{1+\sqrt{1-\frac{U_h^2 C_T}{(\gamma x + U_h)^2}}}dx - \beta\int_0^{l_{nw}} \frac{1}{1+\frac{1}{\sqrt{1-\frac{U_h^2 C_T}{(\gamma x + U_h)^2}}}}dx. \tag{12}$$

The above equation is solved analytically using MATLAB to obtain the near wake length l_{nw}. To solve for l_{nw}, we need to specify the wake width σ_{nw}. Here, we take the σ_{nw} for zero pressure gradient from the experiments, whereas the wake width for different pressure gradient situations is obtained using the invariant ratio. While solving Eq. (12), all the velocities are normalized by U_h in the respective cases and all the distances are normalized by the rotor diameter d. This is done to account for the difference in the reference velocity U_h between different cases while computing the invariant ratio. Finally, the values for model constants (α and β) need to be specified. Here, we choose $\alpha = 0.58$ and $\beta = 0.077$, which are the same values as suggested by Bastankhah and Porté-Agel.[49] However, the α and β values chosen here may not be universal and further research is needed to find universal values for these constants.

Figure 18 shows a comparison of the near wake length obtained from the experiments and the model. Overall, it can be observed that

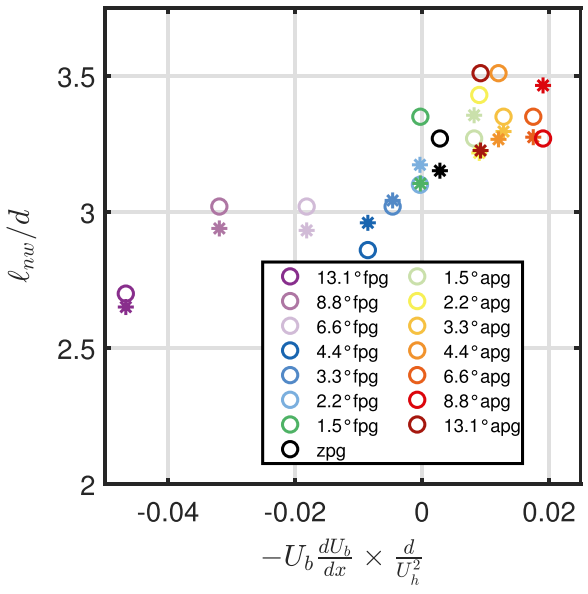

FIG. 18. Comparison of near wake length obtained from the experiments (circles) and the theoretical model (asterisks).

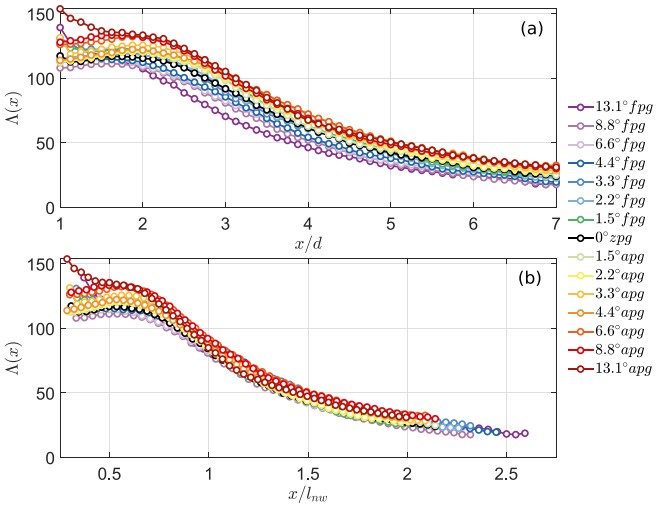

FIG. 19. Comparison of the experimentally obtained invariant ratio with the downstream distance normalized by the rotor diameter (a) and the near wake length (b).

the model can predict the trend between the near wake length and imposed pressure gradient with a very good accuracy. The predicted values are also very close to the experimental ones. Thus, we have derived and validated a theoretical model to estimate the near wake length under an imposed pressure gradient. For the prediction of wake velocity deficit under pressure gradient, we will use this newly derived theoretical near wake length to transition from the near wake solution to the far wake one.

In previous studies,[29,32] the invariant ratio $\Lambda = \frac{CU_b}{\sigma}$ has been verified under the conditions where the far wake is exposed to a pressure gradient. Here, we check its validity under the condition when the turbine experiences a pressure gradient from the induction region to the far wake. Figure 19(a) shows the invariant ratio obtained experimentally for different pressure gradients as a function of downstream distance normalized by the rotor diameter. It is observed that the invariant ratio shows a spread between different pressure gradient cases for $x/d < 4$, beyond which it converges to similar values for all the cases. The spread in the invariant ratio for $x/d < 4$ can be attributed to the difference in the near wake length between different pressure gradient cases. In fact, it can be seen in Fig. 19(b) that normalizing the downstream distance with the near wake length leads to a near-perfect collapse of the invariant ratio in the far wake. We may, therefore, state that the invariant ratio holds when properly accounting for the difference in near wake length caused by the pressure gradient. A similar idea has been recently proposed by Vahidi and Porté-Agel,[56] who showed that turbine wake deficit in flat terrain under different turbulence intensities collapses on a single profile when scaled with respect to the near wake length.

For the pressure gradient model, the invariant ratio under ZPG Λ_0 is obtained from the standard Gaussian model. The invariant ratio in the far wake is used as an input for the estimation of the far wake maximum normalized averaged velocity deficit and wake width for different pressure gradient cases. Figure 20 shows a comparison of the experimentally obtained $C(x)$ and $\sigma(x)/d$ with that obtained from the pressure gradient model. A remarkable improvement over the standard Gaussian model is observed, demonstrating the importance of a physics-based analytical model for wakes under the pressure gradient. Overall, the maximum normalized averaged velocity deficit and normalized wake width show good agreement between the experiments and the pressure gradient model for all the cases. In a few cases, $C(x)$ at the starting point of the pressure gradient model is slightly shifted from the experimental value. This is due to the difference in the experimental and theoretical near wake length estimation. This difference is also observed to decrease with the increase in the downstream distance, as further downstream the model is less sensitive to the chosen near wake length. In fact, if the model is run with the experimental near wake length as an input, the differences between the model and the experiments disappear (figure not shown for the sake of brevity). However, the theoretical near wake length is more useful for practical applications, and it can be stated that the model yields reasonable results for both $C(x)$ and $\sigma(x)/d$.

Finally, Fig. 21 compares the vertical profiles of the normalized averaged streamwise velocity deficit between the experiments, the standard Gaussian model and the pressure gradient model at several downstream distances. It can be seen that the pressure gradient model predicts well the experimental results and offers a significant improvement over the standard Gaussian model, which over (under)-predicts the streamwise velocity deficit for FPG (APG) cases at moderate and high inclination angles. Therefore, we have demonstrated that the pressure gradient model is the better option to analytically model wakes under pressure gradient compared to the engineering approach of superposing the standard Gaussian model on a varying base flow.

IV. SUMMARY AND CONCLUDING REMARKS

Changes in terrain elevation or surface roughness can impose a pressure gradient on the flow, which has a significant effect on the

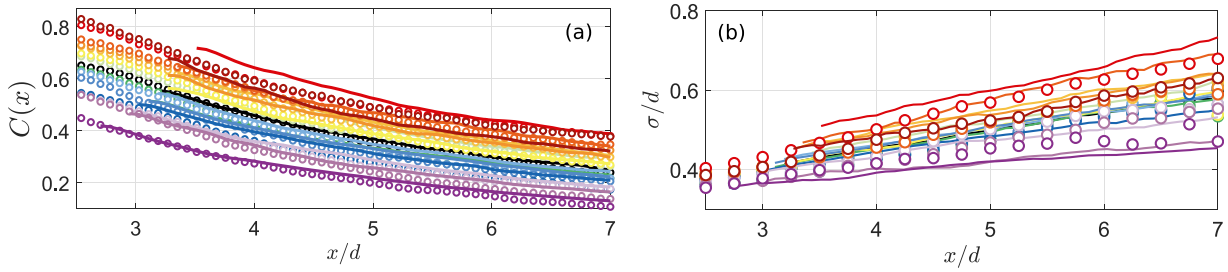

FIG. 20. Comparison of the (a) normalized averaged maximum streamwise velocity deficit $C(x)$ and (b) the normalized wake width obtained from the pressure gradient model (solid lines) and the experiments (circles) for different imposed pressure gradients. The color scheme is the same as Fig. 16.

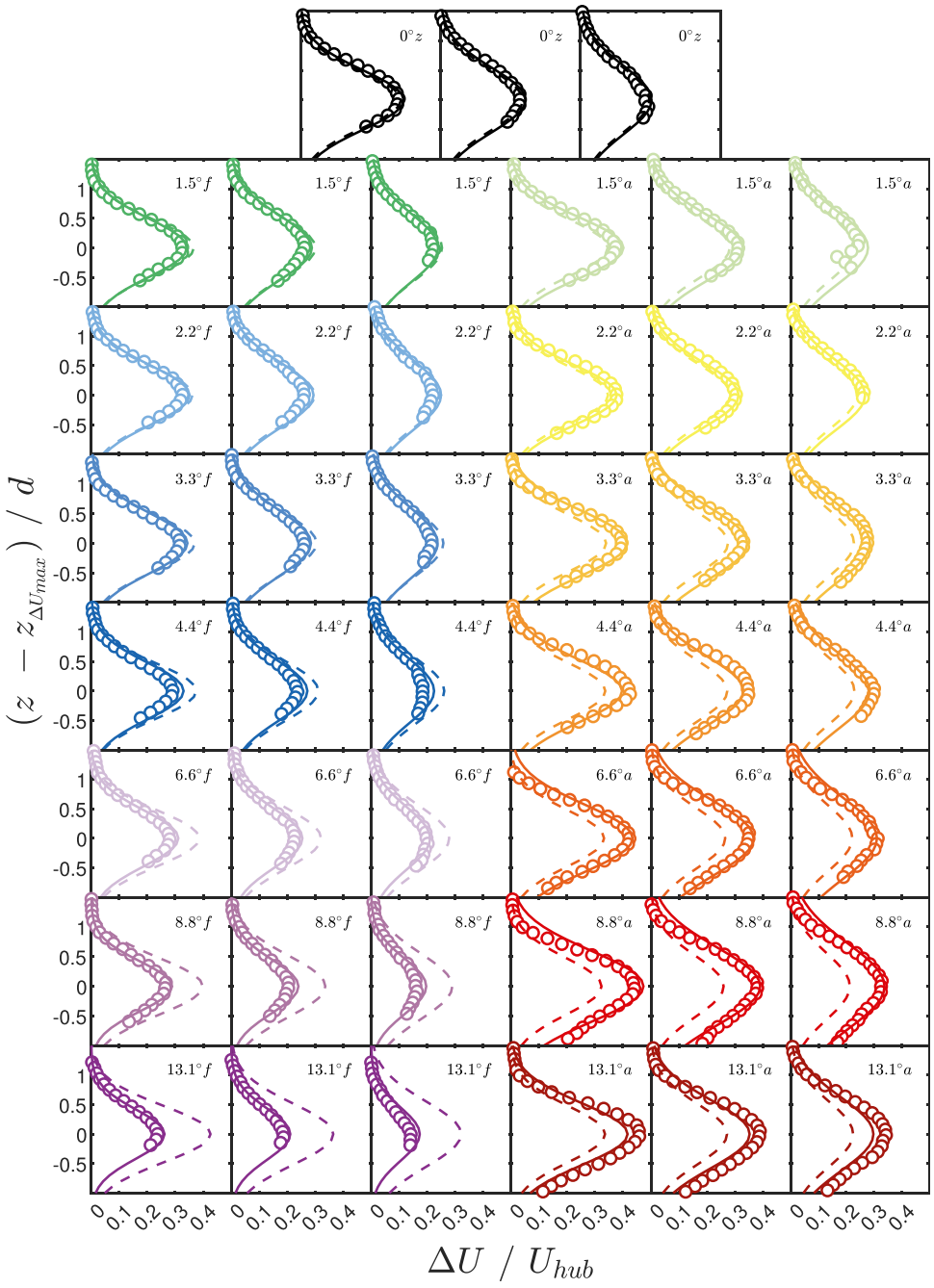

FIG. 21. Comparison of the normalized averaged streamwise velocity deficit profiles obtained from the experiments (circles), the standard Gaussian model (dashed lines), and the pressure gradient model (solid lines) for different imposed pressure gradients. The profiles are shown for $x/d = 5, 6, 7$.

evolution of wind turbine wakes. In this study, we performed a systematic investigation of a wind turbine under an imposed pressure gradient. Wind tunnel experiments were carried out, where flow measurements were made using a planar PIV setup. The pressure gradient was imposed by means of ramps, where the slope of the ramp was varied to impose different pressure gradients. The turbine was placed sufficiently away from the ramp edges such that it experiences an approximately linear flow speed-up/slow-down from its induction region to the far wake. The ramp angle was varied at 15 different inclinations to produce a range of pressure gradients. Seven adverse pressure gradients were produced with inclinations from $-13.1°$ to $-1.5°$, seven favorable from $1.5°$ to $13.1°$, and one zero pressure gradient case at $0.0°$. In the following, we briefly re-address the research questions set out at the beginning of the article.

The experimental results showed a clear systematic relation between the imposed pressure gradient and both the wind turbine

performance and wake characteristics. The power coefficient showed a non-linear dependence on the pressure gradient, with a decrease of up to 9.7% for the strongest adverse pressure gradient, whereas a gain of 6.7% was observed for the strongest favorable pressure gradient. The wake velocity deficit was strongly correlated with pressure gradient—its recovery slowed down with an increase in the adverse pressure gradient and was enhanced by an increase in a favorable pressure gradient. A difference between the wake recovery under the pressure gradient and the zero pressure gradient was computed, which showed some variation in the near wake before reaching a constant value in the far wake. This was related to the difference in the near wake length for different pressure gradient situations. The effect of the pressure gradient on near-to-far wake transition has remained unanswered in the literature. In the current work, we showed that the near wake length is approximately linearly dependent on the imposed pressure gradient, with a decrease (increase) in the near wake length for a favorable (adverse) pressure gradient compared to the zero pressure gradient situation. This was related to the fact that an accelerating base flow results in a faster growth of the shear layer, leading to a shorter near wake length and vice versa. We also showed that the rate of cross-stream expansion of the wake varied linearly as a function of the imposed pressure gradients in our study.

The experimental data were then used to assess different analytical modeling approaches for prediction of wake velocity deficit. In this

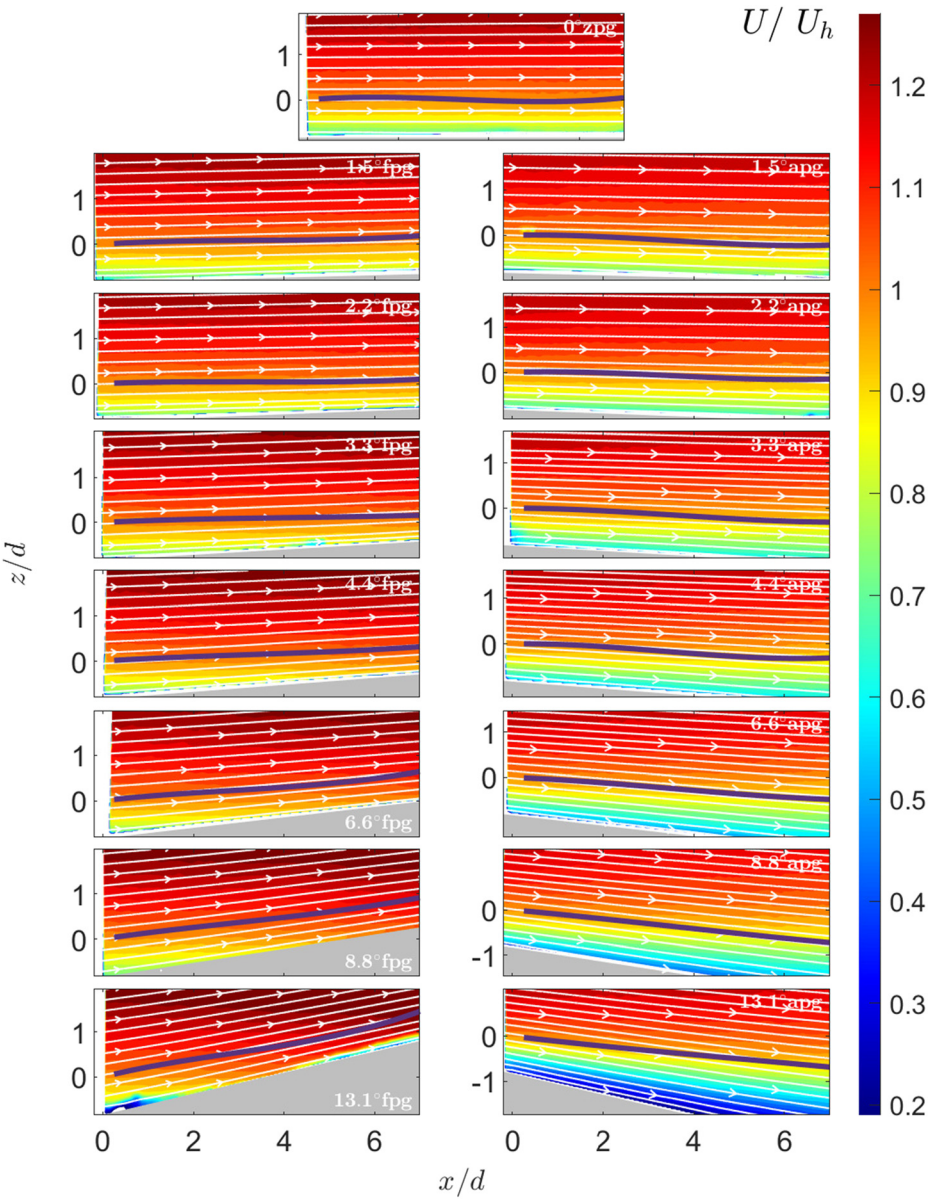

FIG. 22. Contours of the normalized averaged streamwise velocity in the base flow for different pressure gradient conditions. The streamlines of the horizontal and vertical velocity components are overlaid on the contours. The dark solid lines show the wake trajectory For two column panels, the left one corresponds to FPG and the right one corresponds to APG.

context, we first assessed the engineering approach of superposing the streamwise velocity deficit obtained from a zero pressure gradient model on the base flow obtained under the pressure gradient. This approach is currently the most popular one for practical applications. However, we showed that such an approach has serious limitations, as it only worked for moderate pressure gradient situations. We established a threshold in terms of the flow speed-up/slow-down along the wake trajectory up to which the approach yielded acceptable results. This threshold was found to be a speed-up/slow-down of the base flow by 0.57%–0.59% per rotor diameter along the wake center trajectory. We recommend that this threshold must be monitored before applying the standard Gaussian model to pressure gradient situations.

Finally, we showed that a physics-based model developed for wind turbine wakes under the pressure gradient can provide accurate wake deficit prediction. Existing physics-based models provide relations for near/far-wake maximum wake velocity deficit and wake width under pressure gradient situations. However, analytical relations for near wake length under the pressure gradient were lacking. In this context, we derived an analytical relation for the near wake length based on the growth of a shear layer around the rotor periphery. The analytical relation was validated with the experimental data and integrated in the physics-based model to predict the wake velocity deficit under the pressure gradient. The approach was shown to yield excellent results and significantly outperform the engineering approach described earlier. We, therefore, strongly recommend the use of a physics-based analytical model for practical applications involving even moderate pressure gradients, instead of the common engineering approach.

ACKNOWLEDGMENTS

This research was funded by the Swiss National Science Foundation (Grant Numbers: 200021_172538 and 200021_215288) and the Swiss Federal Office of Energy (Grant No. SI/502135–01).

AUTHOR DECLARATIONS

Conflict of Interest

The authors have no conflicts to disclose.

Author Contributions

Arslan Salim Dar: Conceptualization (equal); Data curation (supporting); Formal analysis (equal); Investigation (equal); Methodology (equal); Supervision (supporting); Visualization (equal); Writing – original draft (lead). **Abraham Starbuck Gertler:** Conceptualization (equal); Data curation (lead); Formal analysis (equal); Investigation (equal); Methodology (equal); Visualization (equal); Writing – review & editing (supporting). **Fernando Porte-Agel:** Conceptualization (equal); Formal analysis (supporting); Funding acquisition (lead); Investigation (supporting); Methodology (equal); Project administration (lead); Resources (lead); Supervision (lead); Writing – review & editing (lead).

DATA AVAILABILITY

The data that support the findings of this study are available from the corresponding author upon reasonable request.

APPENDIX: WAKE TRAJECTORY AND BASE FLOW

Figure 22 shows the normalized averaged streamwise velocity in the base flow along with flow streamlines and turbine wake trajectory. This figure is supplementary to the discussion in Sec. II B 3 on the wake trajectory. It can be seen that the wake trajectory follows the base flow streamlines originating from the turbine hub position to a good degree of approximation. In situations where wake trajectory is unknown, the base flow streamline originating from the prospective turbine hub position can be employed as a proxy. In most cases, the vertical deviation of the wake trajectory from the hub height streamline is less than $0.05d$ over a horizontal distance of $7d$. In the most extreme APG case, however, a deviation of about $0.2d$ in the vertical direction is observed at a horizontal position of $7d$, which leads to a difference of about 7.5% at $7d$ between the velocity at the wake trajectory and that at the streamline. Following the base flow streamline was in all cases, a significantly better strategy compared to following the projected hub height.

REFERENCES

[1]GWEC, "Global wind report 2022," (Global Wind Energy Council, 2022).
[2]IRENA, *Renewable Power Generation Costs in 2020* (IRENA, 2021).
[3]P. Veers, K. Dykes, E. Lantz, S. Barth, C. L. Bottasso, O. Carlson, A. Clifton, J. Green, P. Green, H. Holttinen *et al.*, "Grand challenges in the science of wind energy," Science **366**, eaau2027 (2019).
[4]F. Porté-Agel, M. Bastankhah, and S. Shamsoddin, "Wind-turbine and wind-farm flows: A review," Boundary-Layer Meteorol. **174**, 1–59 (2020).
[5]R. J. A. M. Stevens and C. Meneveau, "Flow structure and turbulence in wind farms," Annu. Rev. Fluid Mech. **49**, 311–339 (2017).
[6]P. H. Alfredsson and A. Segalini, "Introduction wind farms in complex terrains: An introduction," Philos. Trans. R. Soc. A **375**, 20160096 (2017).
[7]W. Tian, A. Ozbay, W. Yuan, P. Sarakar, H. Hu, and W. Yuan, "An experimental study on the performances of wind turbines over complex terrain," AIAA Paper No. 2013-0612, 2013.
[8]A. Hyvärinen and A. Segalini, "Effects from complex terrain on wind-turbine performance," J. Energy Resources Technol. **139**, 051205 (2017).
[9]L. Liu and R. J. A. M. Stevens, "Effects of two-dimensional steep hills on the performance of wind turbines and wind farms," Boundary-Layer Meteorol. **176**, 251–269 (2020).
[10]X. Han, D. Liu, C. Xu, and W. Z. Shen, "Atmospheric stability and topography effects on wind turbine performance and wake properties in complex terrain," Renewable Energy **126**, 640–651 (2018).
[11]W. C. Radünz, Y. Sakagami, R. Haas, A. P. Petry, J. C. Passos, M. Miqueletti, and E. Dias, "Influence of atmospheric stability on wind farm performance in complex terrain," Appl. Energy **282**, 116149 (2021).
[12]F. I. P. de, S. Sarmiento, J. L. G. Oliveira, and J. C. Passos, "Impact of atmospheric stability, wake effect and topography on power production at complex-terrain wind farm," Energy **239**, 122211 (2022).
[13]N. Troldborg, S. J. Andersen, E. L. Hodgson, and A. Meyer Forsting, "Brief communication: How does complex terrain change the power curve of a wind turbine?," Wind Energy Sci. **7**, 1527–1532 (2022).
[14]E. S. Politis, J. Prospathopoulos, D. Cabezon, K. S. Hansen, P. K. Chaviaropoulos, and R. J. Barthelmie, "Modeling wake effects in large wind farms in complex terrain: The problem, the methods and the issues," Wind Energy **15**, 161–182 (2012).
[15]M. Tabib, A. Rasheed, and F. Fuchs, "Analyzing complex wake-terrain interactions and its implications on wind-farm performance," J. Phys.: Conf. Ser. **753**, 032063 (2016).
[16]D. Astolfi, F. Castellani, and L. Terzi, "A study of wind turbine wakes in complex terrain through RANS simulation and SCADA data," J. Sol. Energy Eng. **140**, 031001 (2018).
[17]A. S. Dar and F. Porté-Agel, "Wind turbine wakes on escarpments: A wind-tunnel study," Renewable Energy **181**, 1258–1275 (2022).

[18]A. S. Dar, G. Armengol Barcos, and F. Porté-Agel, "An experimental investigation of a roof-mounted horizontal-axis wind turbine in an idealized urban environment," Renewable Energy **193**, 1049–1061 (2022).
[19]Z. Zhang, P. Huang, G. Bitsuamlak, and S. Cao, "Large-eddy simulation of wind-turbine wakes over two-dimensional hills," Phys. Fluids **34**, 065123 (2022).
[20]H. Yang, B. Lang, B. Du, Z. Jin, B. Li, and M. Ge, "Effects of the steepness on the evolution of turbine wakes above continuous hilly terrain," IET Renewable Power Gener. **16**, 1170–1179 (2022).
[21]R. Menke, N. Vasiljević, K. S. Hansen, A. N. Hahmann, and J. Mann, "Does the wind turbine wake follow the topography? A multi-lidar study in complex terrain," Wind Energy Sci. **3**, 681–691 (2018).
[22]R. J. Barthelmie and S. C. Pryor, "Automated wind turbine wake characterization in complex terrain," Atmos. Meas. Tech. **12**, 3463–3484 (2019).
[23]Z. Liu, S. Lu, and T. Ishihara, "Large eddy simulations of wind turbine wakes in typical complex topographies," Wind Energy **24**, 857–886 (2021).
[24]A. S. Dar and F. Porté-Agel, "Three-dimensional wind-turbine wake characterization via tomographic particle-image velocimetry," J. Phys.: Conf. Ser. **1618**, 062045 (2020).
[25]L. Liu and R. J. A. M. Stevens, "Effects of atmospheric stability on the performance of a wind turbine located behind a three-dimensional hill," Renewable Energy **175**, 926–935 (2021).
[26]P. G. Hill, U. Schaub, and Y. Senoo, "Turbulent wakes in pressure gradients," J. Appl. Mech. **30**, 518–524 (1963).
[27]A. Nakayama, "Curvature and pressure-gradient effects on a small-defect wake," J. Fluid Mech. **175**, 215–246 (1987).
[28]X. Liu, F. O. Thomas, and R. C. Nelson, "An experimental investigation of the planar turbulent wake in constant pressure gradient," Phys. Fluids **14**, 2817–2838 (2002).
[29]F. O. Thomas and X. Liu, "An experimental investigation of symmetric and asymmetric turbulent wake development in pressure gradient," Phys. Fluids **16**, 1725–1745 (2004).
[30]M. M. Rogers, "The evolution of strained turbulent plane wakes," J. Fluid Mech. **463**, 53–120 (2002).
[31]S. Shamsoddin and F. Porté-Agel, "Turbulent planar wakes under pressure gradient conditions," J. Fluid Mech. **830**, R4 (2017).
[32]S. Shamsoddin and F. Porté-Agel, "A model for the effect of pressure gradient on turbulent axisymmetric wakes," J. Fluid Mech. **837**, R3 (2018).
[33]S. Shamsoddin and F. Porté-Agel, "Wind turbine wakes over hills," J. Fluid Mech. **855**, 671–702 (2018).
[34]T. Cai, S. Cheng, A. Segalini, and L. P. Chamorro, "Local topography-induced pressure gradient effects on the wake and power output of a model wind turbine," Theor. Appl. Mech. Lett. **11**, 100297 (2021).
[35]T. Göçmen, P. Van der Laan, P.-E. Réthoré, A. P. Diaz, G. C. Larsen, and S. Ott, "Wind turbine wake models developed at the technical university of denmark: A review," Renewable Sustainable Energy Rev. **60**, 752–769 (2016).
[36]J. K. Kaldellis, P. Triantafyllou, and P. Stinis, "Critical evaluation of wind turbines' analytical wake models," Renewable Sustainable Energy Rev. **144**, 110991 (2021).
[37]N. O. Jensen, "A note on wind generator interaction," Report No. Risø-M-2411, Risø National Laboratory, Roskilde, Denmark (1983).
[38]S. Frandsen, R. Barthelmie, S. Pryor, O. Rathmann, S. Larsen, J. Højstrup, and M. Thøgersen, "Analytical modelling of wind speed deficit in large offshore wind farms," Wind Energy **9**, 39–53 (2006).
[39]M. Bastankhah and F. Porté-Agel, "A new analytical model for wind-turbine wakes," Renewable Energy **70**, 116–123 (2014).
[40]S. Xie and C. L. Archer, "A numerical study of wind-turbine wakes for three atmospheric stability conditions," Boundary-Layer Meteorol. **165**, 87–112 (2017).
[41]A. S. Dar, J. Berg, N. Troldborg, and E. G. Patton, "On the self-similarity of wind turbine wakes in a complex terrain using large eddy simulation," Wind Energy Sci. **4**, 633–644 (2019).
[42]R. Brogna, J. Feng, J. N. Sørensen, W. Z. Shen, and F. Porté-Agel, "A new wake model and comparison of eight algorithms for layout optimization of wind farms in complex terrain," Appl. Energy **259**, 114189 (2020).
[43]A. Farrell, J. King, C. Draxl, R. Mudafort, N. Hamilton, C. J. Bay, P. Fleming, and E. Simley, "Design and analysis of a wake model for spatially heterogeneous flow," Wind Energy Sci. **6**, 737–758 (2021).
[44]A. S. Dar and F. Porté-Agel, "An analytical model for wind turbine wakes under pressure gradient," Energies **15**, 5345 (2022).
[45]M. Bastankhah and F. Porté-Agel, "A new miniature wind turbine for wind tunnel experiments. Part I: Design and performance," Energies **10**, 908 (2017).
[46]B. Wieneke, "PIV uncertainty quantification from correlation statistics," Meas. Sci. Technol. **26**, 074002 (2015).
[47]L. P. Chamorro, R. E. Arndt, and F. Sotiropoulos, "Reynolds number dependence of turbulence statistics in the wake of wind turbines," Wind Energy **15**, 733–742 (2012).
[48]P. Vermeulen, "An experimental analysis of wind turbine wakes," in *3rd International Symposium on Wind Energy Systems* (Lyngby, Denmark, 1980), pp. 431–450.
[49]M. Bastankhah and F. Porté-Agel, "Experimental and theoretical study of wind turbine wakes in yawed conditions," J. Fluid Mech. **806**, 506–541 (2016).
[50]M. Abkar, J. N. Sørensen, and F. Porté-Agel, "An analytical model for the effect of vertical wind veer on wind turbine wakes," Energies **11**, 1838 (2018).
[51]Y.-T. Wu and F. Porté-Agel, "Atmospheric turbulence effects on wind-turbine wakes: An LES study," Energies **5**, 5340–5362 (2012).
[52]X. Fan, M. Ge, W. Tan, and Q. Li, "Impacts of coexisting buildings and trees on the performance of rooftop wind turbines: An idealized numerical study," Renewable Energy **177**, 164–180 (2021).
[53]W. Hu, Q. Yang, H.-P. Chen, K. Guo, T. Zhou, M. Liu, J. Zhang, and Z. Yuan, "A novel approach for wind farm micro-siting in complex terrain based on an improved genetic algorithm," Energy **251**, 123970 (2022).
[54]P. Brugger, F. Fuertes, M. Vahidzadeh, C. Markfort, and F. Porté-Agel, "Characterization of wind turbine wakes with nacelle-mounted doppler lidars and model validation in the presence of wind veer," Remote Sens. **11**, 2247 (2019).
[55]J. H. Lee and V. Chu, *Turbulent Jets and Plumes: A Lagrangian Approach* (Springer Science & Business Media, 2012), Vol. 1.
[56]D. Vahidi and F. Porté-Agel, "A new streamwise scaling for wind turbine wake modeling in the atmospheric boundary layer," Energies **15**, 9477 (2022).